INFORMATION TO USERS

This was produced from a copy of a document sent to us for microfilming. While the most advanced technological means to photograph and reproduce this document have been used, the quality is heavily dependent upon the quality of the material submitted.

The following explanation of techniques is provided to help you understand markings or notations which may appear on this reproduction.

1. The sign or "target" for pages apparently lacking from the document photographed is "Missing Page(s)". If it was possible to obtain the missing page(s) or section, they are spliced into the film along with adjacent pages. This may have necessitated cutting through an image and duplicating adjacent pages to assure you of complete continuity.

2. When an image on the film is obliterated with a round black mark it is an indication that the film inspector noticed either blurred copy because of movement during exposure, or duplicate copy. Unless we meant to delete copyrighted materials that should not have been filmed, you will find a good image of the page in the adjacent frame.

3. When a map, drawing or chart, etc., is part of the material being photographed the photographer has followed a definite method in "sectioning" the material. It is customary to begin filming at the upper left hand corner of a large sheet and to continue from left to right in equal sections with small overlaps. If necessary, sectioning is continued again—beginning below the first row and continuing on until complete.

4. For any illustrations that cannot be reproduced satisfactorily by xerography, photographic prints can be purchased at additional cost and tipped into your xerographic copy. Requests can be made to our Dissertations Customer Services Department.

5. Some pages in any document may have indistinct print. In all cases we have filmed the best available copy.

University
Microfilms
International

300 N. ZEEB ROAD, ANN ARBOR, MI 48106
18 BEDFORD ROW, LONDON WC1R 4EJ, ENGLAND

HOLMES, ALAN WRIGHT

LIGHT SCATTERING FROM AMMONIA AND WATER CRYSTALS

The University of Arizona PH.D. 1981

PLEASE NOTE:

In all cases this material has been filmed in the best possible way from the available copy. Problems encountered with this document have been identified here with a check mark __✓__.

1. Glossy photographs or pages ✓
2. Colored illustrations, paper or print _____
3. Photographs with dark background ✓
4. Illustrations are poor copy _____
5. Pages with black marks, not original copy _____
6. Print shows through as there is text on both sides of page _____
7. Indistinct, broken or small print on several pages ✓
8. Print exceeds margin requirements _____
9. Tightly bound copy with print lost in spine _____
10. Computer printout pages with indistinct print _____
11. Page(s) _____ lacking when material received, and not available from school or author.
12. Page(s) _____ seem to be missing in numbering only as text follows.
13. Two pages numbered _____. Text follows.
14. Curling and wrinkled pages _____
15. Other _____

LIGHT SCATTERING FROM AMMONIA AND WATER CRYSTALS

by

Alan Wright Holmes

A Dissertation Submitted to the Faculty of the

COMMITTEE ON OPTICAL SCIENCES (GRADUATE)

In Partial Fulfillment of the Requirements
For the Degree of

DOCTOR OF PHILOSOPHY

In the Graduate College

THE UNIVERSITY OF ARIZONA

1 9 8 1

THE UNIVERSITY OF ARIZONA
GRADUATE COLLEGE

As members of the Final Examination Committee, we certify that we have read the dissertation prepared by Alan Wright Holmes

entitled Light Scattering from Ammonia and Water Crystals

and recommend that it be accepted as fulfilling the dissertation requirement for the Degree of Doctor of Philosophy.

Donald R. Huffman	March 13, 1981 Date
Martin G. Tomasko	3/13/81 Date
W. W. Wolfe	3/13/81 Date
	Date
	Date

Final approval and acceptance of this dissertation is contingent upon the candidate's submission of the final copy of the dissertation to the Graduate College.

I hereby certify that I have read this dissertation prepared under my direction and recommend that it be accepted as fulfilling the dissertation requirement.

W. W. Wolfe
Dissertation Director

3/13/81
Date

STATEMENT BY AUTHOR

This dissertation has been submitted in partial fulfillment of requirements for an advanced degree at The University of Arizona and is deposited in the University Library to be made available to borrowers under rules of the Library.

Brief quotations from this dissertation are allowable without special permission, provided that accurate acknowledgment of source is made. Requests for permission for extended quotation from or reproduction of this manuscript in whole or in part may be granted by the head of the major department or the Dean of the Graduate College when in his judgment the proposed use of the material is in the interests of scholarship. In all other instances, however, permission must be obtained from the author.

SIGNED: Alan Holmes

ACKNOWLEDGMENTS

This work could not have been accomplished without the advice and patient assistance of many people. Dr. Martin Tomasko motivated the initiation of this research and Professor W. Wolfe provided guidance and laboratory equipment essential to its completion. Dr. Donald Huffman recommended the computerized approach employed here and contributed many hours of fruitful discussions concerning experimental technique. Many thanks are deserved by Rick Paxman and Phil Stahl for their help and suggestions. A special thanks goes to Paulette Vashio for reminding me throughout this research that there is something else in life besides optics. Barbara Bickel's help was invaluable in preparing this manuscript. I am also grateful to my fellow workers in the Infrared Lab for their suggestions, their interest, and their patience in enduring many hours in a darkened laboratory permeated with the smell of ammonia!

TABLE OF CONTENTS

TABLE OF CONTENTS--Continued

LIST OF ILLUSTRATIONS

LIST OF ILLUSTRATIONS--Continued

LIST OF TABLES

ABSTRACT

Researchers analyzing the upper clouds of Jupiter and Saturn are unable to theoretically reproduce the data returned by Pioneers 10 and 11 and Voyagers 1 and 2 with an approach based on Mie theory. Ammonia crystals are believed to be an important constituent of Jupiter's upper clouds, but both their shape and scattering properties were unknown at the start of this work.

Ammonia crystals and water crystals were grown in a cold chamber at temperatures 20°C below their freezing points (0°C and -77.7°C, respectively). The H_2O crystals formed had shapes in agreement with published growth habit diagrams. The NH_3 crystals formed were usually irregular in shape, but regular four-sided pyramids were commonly observed. This four-sided pyramidal shape is in agreement with ammonia's primitive cubic crystal structure. Ammonia crystals could not be formed at temperatures above -95°C due to nucleation problems.

A scattering measuring instrument was constructed with fifteen separate lens-detector combinations aimed at a common point in the center of the cold chamber. A laser beam (6328Å wavelength) traversed the chamber center, illuminating any crystal aerosol clouds present. A computer was used to rapidly sample the outputs of the fifteen detectors and to drive a photoelectric modulator to change the slow speed polarization properties of the laser beam. The measurements resulted in a determination of the single scattering phase function and degree of linear polarization for the crystal species present.

Water crystals were found to have scattering properties similar to that reported by previous researchers. The H_2O crystal scattering possesses a smaller backscatter peak and smaller polarization features than is common for water spheres of similar size. A negative polarization of 5% occurred in the forward scattering hemisphere and a positive polarization of 10% in the rear.

Ammonia particles were observed to have a backscattering peak four times higher than for water crystals. The NH_3 particle light scattering produced very little polarization of the scattered light. A small ($\sim$ 4%) negative polarization occurred in the forward scattering hemisphere.

Work is continuing here to make scattering measurements using blue light illumination nearly simultaneous with the red HeNe laser wavelength illumination.

CHAPTER 1

INTRODUCTION

The subject of light scattering by water and ammonia crystals has acquired recent interest from investigators studying the upper clouds of the earth, Jupiter, and Saturn. The flybys of Jupiter and Saturn by Pioneers 10 and 11 and Voyagers 1 and 2 produced a wealth of information concerning observable features of the cloud bands. These probes all carried polarimeters to measure the brightness and degree of polarization of sunlight reflected from the clouds at a variety of Sun-Jupiter-probe angles. The Voyager probe polarimeters suffered a malfunction which rendered them inoperable, but the data from the Pioneer probes alone will occupy researchers for years. These theoreticians, specifically Tomasko, West, and Castillo (1978), have already found that they could not reproduce the observed light scattering properties of the upper cloud decks of Jupiter using an analysis based on Mie theory, which assumes the scattering particles are spherical. Their analysis of the multiply scattered radiation from the cloud decks led them to the hypothesis that the particles are crystalline in nature, with ammonia crystals being the most likely candidate. Tomasko et al. (1978) noted that no general theory of scattering by crystalline objects of size comparable to the wavelength of visible light exists and suggested that an experiment to measure the scattering of light by plausible crystal

species would help fill this void. It is to this end that this experimental study represents a beginning, a hope to recover more information from the millions of dollars and thousands of man hours of analysis devoted to this study of planetary atmospheres. The goal of this experimental study is to reproduce the atmosphere of Jupiter in a laboratory cold chamber, grow crystals of ammonia and water, and characterize their shapes, sizes and light scattering properties. This report concerns itself with the realizations of this goal, and the results obtained.

Experimental Goals

The first goal of this project is to grow H_2O and NH_3 crystals from the vapor and to characterize the shape and size distributions of the crystals that are formed. The capability was desired of accomplishing this goal over a range of temperatures and pressures. The second major goal of this project is to measure the scattering properties of these crystals using red light illumination, specifically He-Ne laser light with a wavelength of 0.632 microns. The scattering properties chosen for measurement were the single scattering phase function and the degree of linear polarization. The angular resolution of the measurements of these functions is adequate for comparison to the Pioneer data.

Limitations of the Current Research

Some limitations of the applicability of this research to the reduction of Pioneer spacecraft data do exist. The gas in which the crystals were grown in this experiment was nitrogen whereas hydrogen would be more accurate in reproducing Jupiter's upper atmosphere. Also,

the colors of Jupiter's upper cloud decks are caused by trace impurities of unknown composition, which may affect crystal scattering properties. No attempt is made here to reproduce these effects. The scattering measurement done here is confined to the horizontal plane for experimental reasons while the scattering from Jupiter is more similar to measurements made in the vertical plane (with respect to gravity). This does not result in an error if the crystals are randomly oriented as they fall.

CHAPTER 2

CRYSTAL PRODUCTION

The process whereby clouds of ice crystals form in nature is fundamentally simple and is described in introductory atmospheric physics texts. The process, summarized in Figure 1, begins with a parcel of gas moist with ammonia or water being warmed by some heat source and rising.

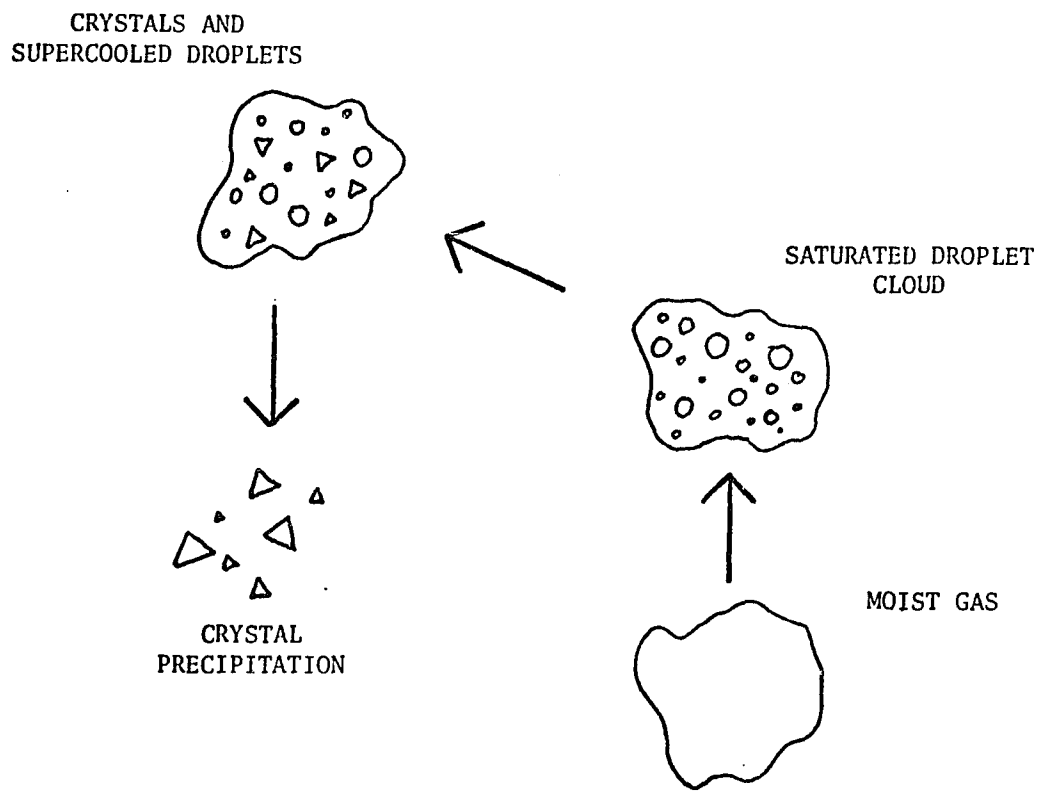

Figure 1. Summary of Meteorological Cloud Formation Process.

As it rises this parcel cools adiabatically and becomes saturated with respect to the precipitable component. After this point further cooling causes the excess moisture to condense out as a fog of small cloud droplets. As the parcel of gas rises further, the cloud droplets supercool, i.e., the temperature of the drops falls below the freezing point of the bulk liquid. This phenomenon is rarely observed on earth for large quantities of water, but it is not unusual for cloud droplets to supercool to as much as -40°C. If ice nucleation particles exist in the supercooled cloud, ice crystals will begin to form. The vapor pressure over the solid ice is less than that over the liquid water and the crystals will grow at the expense of the droplets. When the crystals become large, gravity pulls them down from the clouds.

Two important points of this process need more explanation. Condensation nuclei must exist for the droplets to form as the gas parcel becomes slightly supersaturated. These nuclei are quite common in the earth's atmosphere and are thought to be soluble particles such as sea salt aerosols. Ice crystal nuclei must exist for ice crystals to be formed in a modestly supercooled (and therefore supersaturated with respect to ice) droplet cloud. Ice crystal nuclei are relatively rare in the earth's atmosphere, being only about one per liter at a temperature of -20°C. These particles are thought to be mostly insoluble in water. It is apparent from this small number that "seeding" of the droplet clouds must be done in small chambers to get appreciable crystal densities. Silver iodide is a common agent for seeding water clouds, and none is known for ammonia.

Experimental Difficulties with Growing Ice Crystals

The fundamental advantage nature has over laboratory techniques for growing clouds is that nature has kilometers of room. Modest experimental budgets limit the growing volume to at best a few cubic meters. Many of the initial researches on ice crystals were done in large food lockers or Air Force test chambers (Huffman and Thursby, 1969; Dugin et al., 1971). The scattering machinery was often located inside the chamber and operated by a parka-clad experimentalist. This approach was deemed too severe to employ for ammonia, since it would have required a student to work in a -120°C chamber while wearing a full face gas mask. Also, it was necessary to locate experimental gear external to the chamber. These problems all make a small chamber most attractive, but the proximity of the walls to the gas makes cloud formation more difficult and creates the problems listed below:

a) Any temperature difference between the gas and the walls will cause swift convection currents to flow.

b) Windows in the chamber can frost in the presence of a cloud of saturated vapor.

c) A supercooled cloud is not stable as the chamber walls frost, pulling in the excess vapor.

d) The humidity in the chamber will come to equilibrium with the coldest surface in the chamber. Since gas diffusion is a faster process than temperature equilibration, the gas can never reach stability at 100% saturation in the presence of temperature variations.

It is apparent from these considerations that it can be difficult to create a stable, long lasting cloud in a laboratory situation. The two most common approaches for forming clouds are the adiabatic expansion and the gaseous diffusion techniques. In the adiabatic expansion chamber a quantity of gas becomes saturated by the presence of moisture. The pressure is then suddenly decreased and the associated cooling of the gas produces an immediate supersaturation. Droplets form and, at lower temperatures, ice crystals grow. The gaseous diffusion chamber produces this necessary supersaturation by a different technique. A cloth reservoir soaked with the liquid or ice of interest is located in the top of the chamber. A quantity of gas is allowed to reach saturation in the presence of this moisture. A wire embedded in the cloth reservoir is then resistively heated and vapor driven off. This vapor diffuses rapidly into the chamber, producing a supersaturated region in the vicinity of the wire. Precipitation is then possible.

These techniques suffer from an uncertainty of the exact temperature of crystal formation because both produce temperature variations, also causing convection currents. In the diffusion chamber, the stirring by convection currents can be minimized as the source of heat is at the top of the chamber. The chamber built for this study can be used either way, but has been most successfully employed in the diffusion chamber mode.

The Cold Chamber

A chamber was developed and constructed for the purpose of growing and observing water and ammonia crystals. The necessity for

operation at temperatures well below the freezing point of NH_3, -77.7°C, dictated many aspects of the chamber design. The chamber is illustrated in Figure 2 alongside a scale to reveal its small size.

The inner chamber, possessing a volume of 60 cc, is shielded from the room-temperature environment by vacuum on all sides, with gas transfer tubes constructed of stainless steel bellows to minimize heat transfer. The chamber is constructed of aluminum, which is resistant to corrosion by ammonia. The aluminum is used in thick cross sections to minimize temperature variations in the chamber walls. Epoxies were used for permanent joint seals and silicone rubber RTV-560 for breakable seals around the lower microscope cover glass window and lower securing screws. The inner chamber is cooled with a brass ring thermally connected through an indium gasket. The brass ring itself is cooled by liquid nitrogen poured in through bellows from above. The curved inner windows were sealed with an external o-ring developed by Parker O-ring company for operation at temperatures down to -125°C. The outer cylindrical window and other warm seals were easily sealed with o-rings. As a whole, the system never held an excellent vacuum due to unidentified leaks in the inner chamber that "healed" at warm temperatures, but it has been satisfactory under continuous pumping.

The laser beam passes through the chamber at a height of 9.5 mm above a microscope cover glass upon which precipitable particles can be observed. The beam is absorbed by a simple cylindrical light trap after illuminating the scattering volume. The microscope objective directly under the cover glass is focused on the glass by rotation in a fine threaded mount. The objective is well-connected thermally to the lower

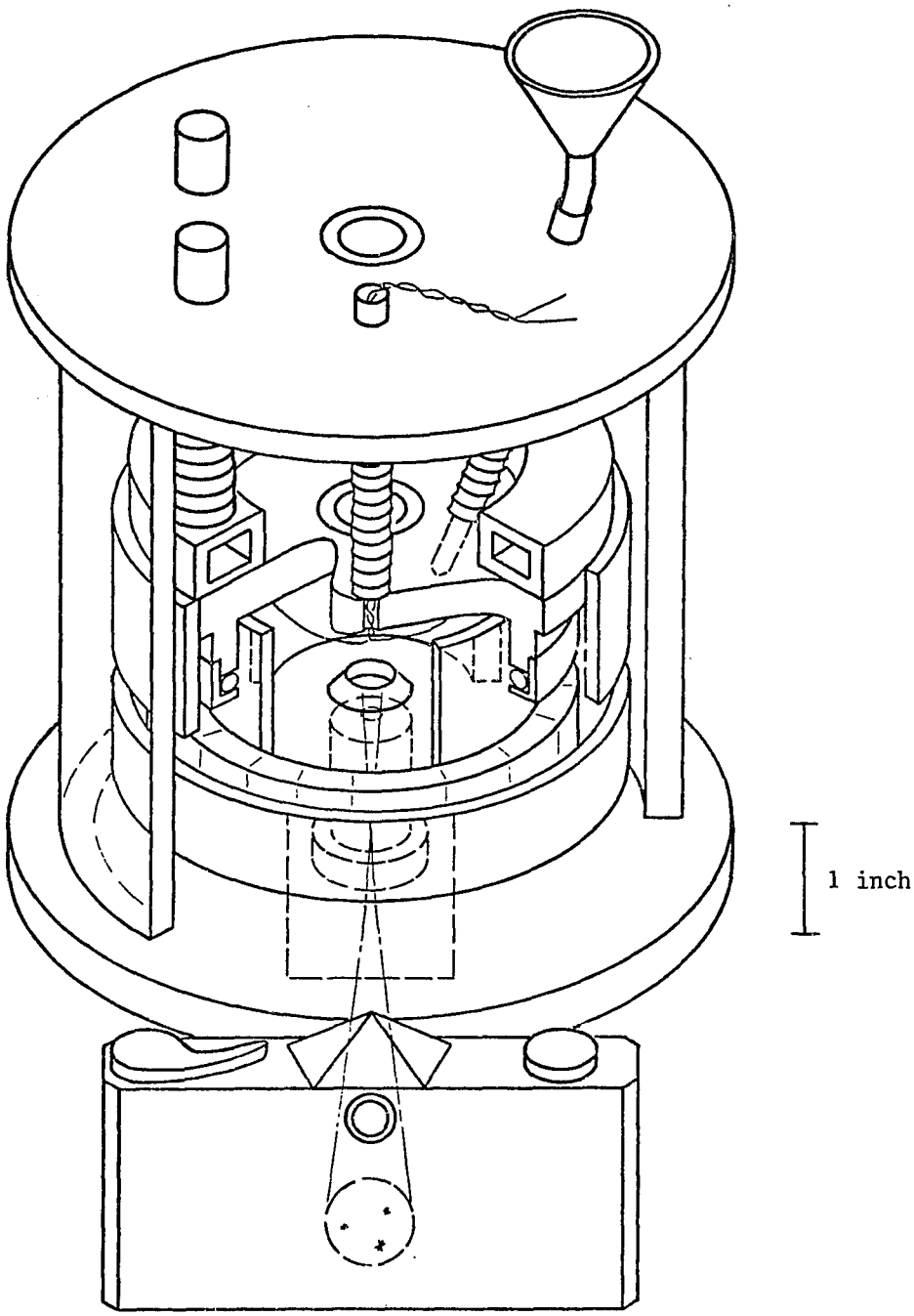

Figure 2. Cold Chamber Diagram.

aluminum base plate and as a result radiates some heat to the microscope cover glass. The particles that fall on the cover glass are illuminated by a microscope illuminator above the chamber, the light passing through two windows. The optical resolution of this photomicrography system is about one micron at temperatures of -110°C.

Technique for Crystal Growth

Crystals were grown in the chamber by the procedure described below. Liquid nitrogen was poured repetitively into the hollow brass ring until the inner chamber cooled to a temperature a few degrees above the freezing point of ammonia. Gas was then slowly admitted into the chamber. The ammonia gas liquefied upon passing through the cold stainless steel bellows tubes and wet a fiberglass sheath surrounding a nichrome wire loop in the top of the chamber. The chamber was then cooled further. At the chosen operating temperature the chamber was allowed to stabilize for ten minutes. A cold finger constructed of a hollow stainless steel tube blocked at the bottom was permanently installed in the chamber such that the lower end protruded one-quarter inch into the top of the chamber. This cold finger, when cooled by a small quantity of liquid nitrogen, caused the chamber to fill with a fog of small particles. This fog slowly dissipated, and when it had almost disappeared, an electric current was passed through the nichrome wire thereby heating the sheath and driving ammonia vapor into the chamber. This vapor diffused into the cold gas and caused the few remaining ice particles, which acted as seeds, to grow rapidly. These

particles precipitated out in a matter of 60 seconds, and the chamber returned to its initial state.

Water crystals were grown in a similar fashion, the important difference being that the fiberglass sheath was wet with water applied with a hypodermic needle. The crystals that resulted are illustrated in Chapter 3 and are consistent with published data on the growth habit of water crystals grown at large supersaturations. This fact builds confidence in the assumption that crystal growth takes place at a temperature only slightly above that of the chamber wall.

The clouds that were formed in the cold chamber were generally quite dense. The convection currents that accompanied the cooling of the cold finger and the heating of the fiberglass sheath helped stir the chamber gas, producing a quasi-uniform cloud. These currents were downward in the middle of the chamber, bringing crystals directly through the laser beam and onto the microscope cover glass. This fortuitous churning of the currents was the result of many hours of trial-and-error.

Effect of Water Contamination on Chamber Performance

There are no problems associated with water contamination in the growth of water ice crystals but only in the growth of ammonia crystals. Slight amounts of room air can be pulled into the chamber at very cold temperatures by vacuum leaks or injected by attempts to flush the chamber volume with ultra-dry nitrogen that has passed through tubes which outgas moisture. In either case, the net effect is that a thin fog of very small particles can appear in the chamber at temperatures from -40°C down to the chamber limit of -120°C. The deleterious effects

of this fog can be understood by examining Figure 3, which was drawn from data contained in the International Critical Tables (1928) and from J. S. Lewis (1969).

Ammonia is capable of forming two stable hydrates with water, $2NH_3 \cdot H_2O$ and $NH_3 \cdot H_2O$. These hydrates would require more water than was probably leaking into the chamber and most likely did not occur. Note that the freezing point could be depressed as low as -100°C if they did occur. What is more probable is that the water crystals serve as condensation nuclei for ammonia, producing drops which are in the neighborhood of 95% ammonia by weight. These drops will have a vapor pressure lower than pure liquid ammonia by an amount comparable to frozen ammonia

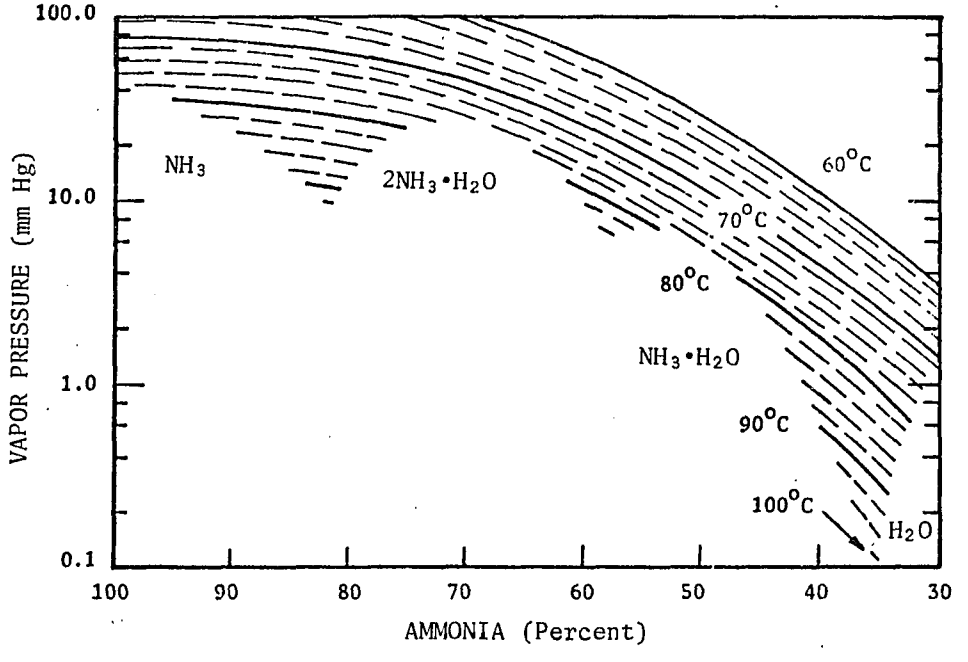

Figure 3. Vapor Pressure over Ammonia, Water, and Two Hydrates of Ammonia. -- Note the freezing point depression possible under different conditions.

and will compete with the crystals for the available excess vapor. These contaminated droplets are more stable with vapor pressure fluctuations, also. If the ammonia partial pressure drops slightly, ammonia will evaporate out of the solution drops and a new equilibrium will be established at a slightly smaller ammonia-to-water ratio. At the low temperatures involved, water effectively has no vapor pressure.

The observed effect of water contamination was the presence of long-lived fogs in the chamber that did not settle out in times as long as 30 minutes. Attempts to grow crystals in the presence of these fogs only caused the fog to become denser, scattering more light. This scattered light was quite intense, making a crystal scattering measurement impossible even if crystals could be produced under these perturbing conditions.

This problem is minimized by control of gas flow paths into the chamber. Entrances into the chamber were sealed carefully and a gas reservoir filled with potassium hydroxide established between the chamber and the room air. Any pressure changes or vacuum leaks pull vapor into the chamber through this drying medium at a slow rate and fogs do not occur. The chamber cannot be flushed at a low temperature, but this was not necessary.

Measurement of Crystal Size

Crystals sizes are measured by a tedious examination of photographs of chamber precipitation products with a microscopic eyepiece plus reticle. This procedure is accurate assuming that a representative sample of the scattering particles in the chamber falls to the

microscope cover glass. This is not the case if the chamber is observed to be filled with fog, or if the precipitation particles evaporate before the photographs can be taken. The microscope cover glass seems to be warmed by the presence of the microscope objective. As a result, ammonia crystals striking the cover glass sublimate rapidly at chamber temperatures above -95°C. At these important temperatures, pictures were taken rapidly to insure as accurate a size determination as possible. Water has a lower vapor pressure at its sub-freezing temperatures and sublimation was not a problem.

Scattering measurements and photographs are avoided when the chamber has significant fog levels. Small particles such as fog particles tend to follow convection currents and do not appreciably precipitate out under the influence of gravity.

CHAPTER 3

RESULTS: CRYSTAL SHAPES AND SIZES

Water

Water crystals were grown as described in the previous chapter. No nucleating agent was used. Crystals grown at temperatures far below the freezing point tended to be very small, too small for their shapes to be resolved in the photographs. Figure 4 is an illustration of these unresolved particles that formed at a temperature of -39°C. Larger crystals formed at warmer temperatures with shapes that were in agreement with the published growth habits of water crystals grown under large supersaturations (Byers, 1965). These crystal species are illustrated in Figures 5 and 6. These clouds of plate crystals were produced with the size distribution shown in Figure 7. The mean sizes for the crystals grown at -39°C, -26°C, and -18°C were 3.7 μm, 5.5 μm, and 8.5 μm, respectively. The different scattered light distributions corresponding to these different mean sizes are presented in Chapter 5.

Ammonia

Ammonia crystals were formed at temperatures from -95°C to -120°C. The freezing point of ammonia is -77°C but crystals could not be successfully produced at temperatures above -95°C due to a lack of ice nuclei in the chamber.

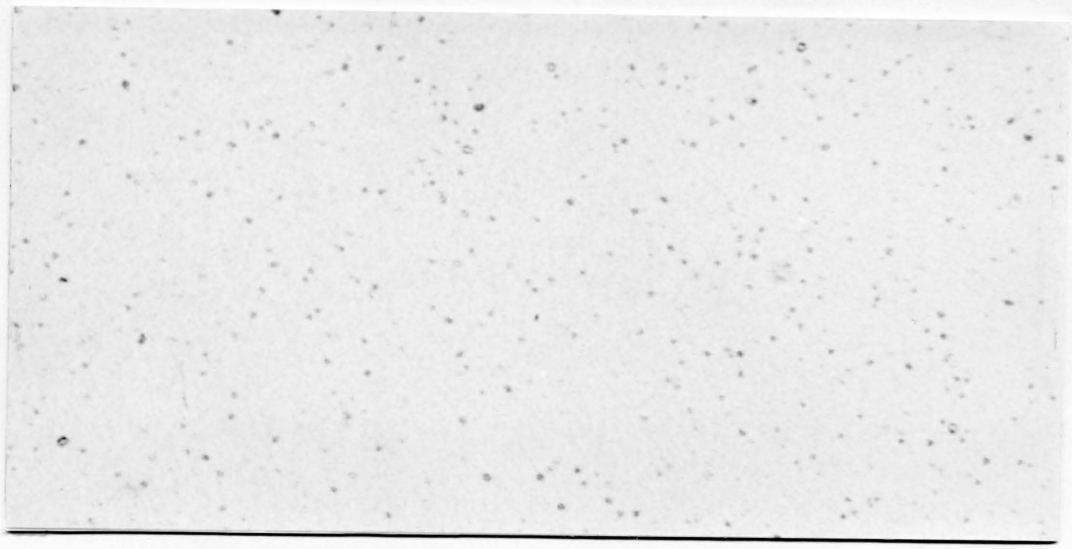

Figure 4. Water Crystals Grown at -39°C.

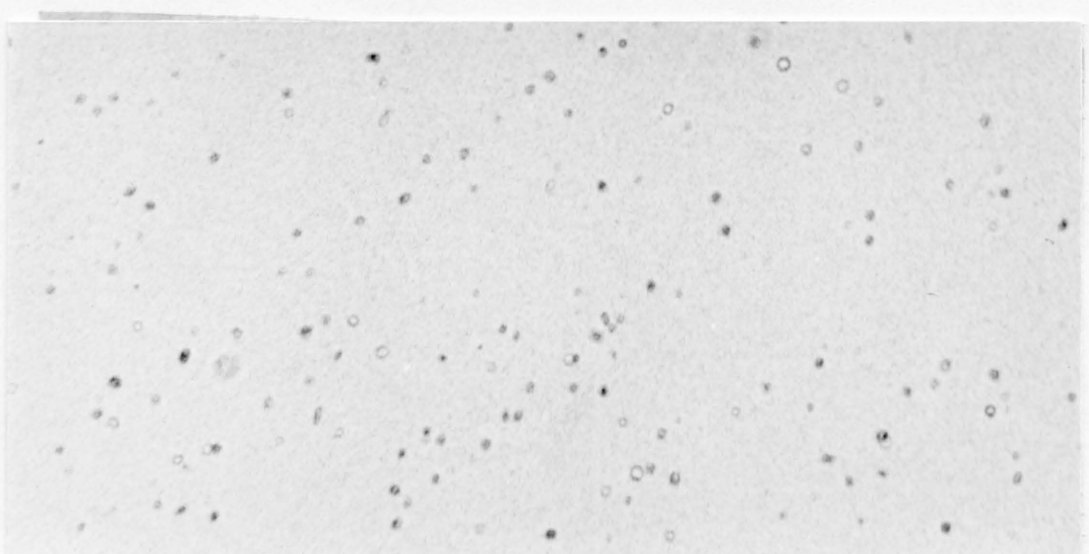

Figure 5. Water Crystals Grown at -26°C.

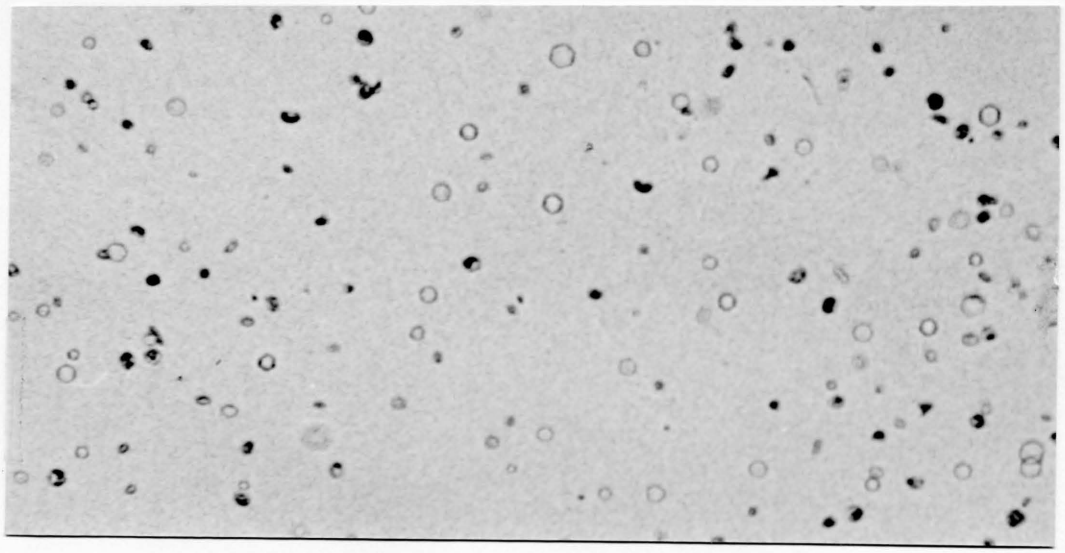

Figure 6. Water Crystals Grown at -18°C.

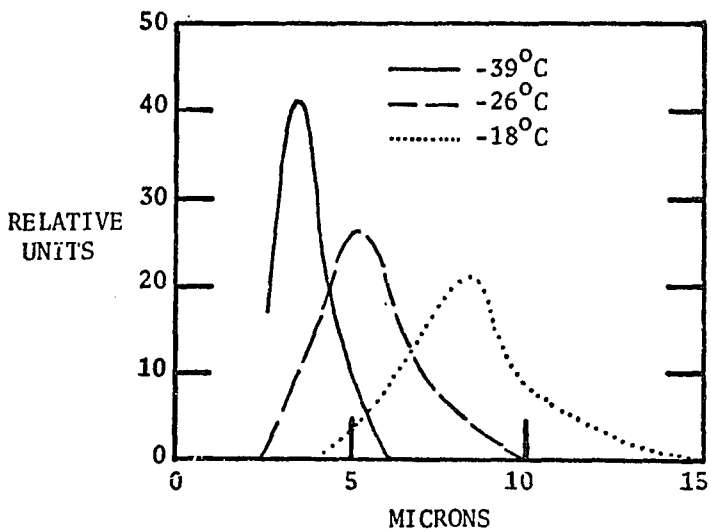

Figure 7. Size Distribution of the Maximum Dimension of the Water Crystals Illustrated in Figures 4, 5, and 6.

Ammonia crystals formed at -98°C showed definite crystal structure in many photographs, as is illustrated in Figure 8. These crystal forms are shown to be compatible with the known primitive cubic structure of solid ammonia (Crystal Data, n.d.) in Figure 9. Rounded objects are seen in many of the photographs of the ammonia precipitation which are apparently the result of multiple nucleation, i.e., a crystal growing from several seeds, resulting in a misshapen crystal (S. A. Twomey, Atmospheric Sciences, University of Arizona, personal communication). Such irregular ice crystal formation occurs in terrestrial clouds and may occur in the atmospheres of other planets. Some of the irregular objects in Figure 8 are four-sided ammonia crystals viewed from different angles. The different apparent shapes possible are illustrated in Figure 10.

Crystals formed at colder temperatures are often linked together in twos and threes, as evidenced in Figure 11. This feature is probably related to the large excess vapor pressure of ammonia produced by the moist wire heater. This excess vapor produces denser clouds of crystals than occur at warmer temperatures, thereby increasing the probability of two particles undergoing a collision and sticking. The formation of chain-like groups was shown to be statistically probable by Sutherland (1970).

The size distribution of the crystals is given in Figure 12. The mean size for the two temperatures, -98°C and -117°C, was 6.3 μm and 7.5 μm, respectively. The mean size given for crystals formed at -117°C refers to the individual particles that form the chains or clumps.

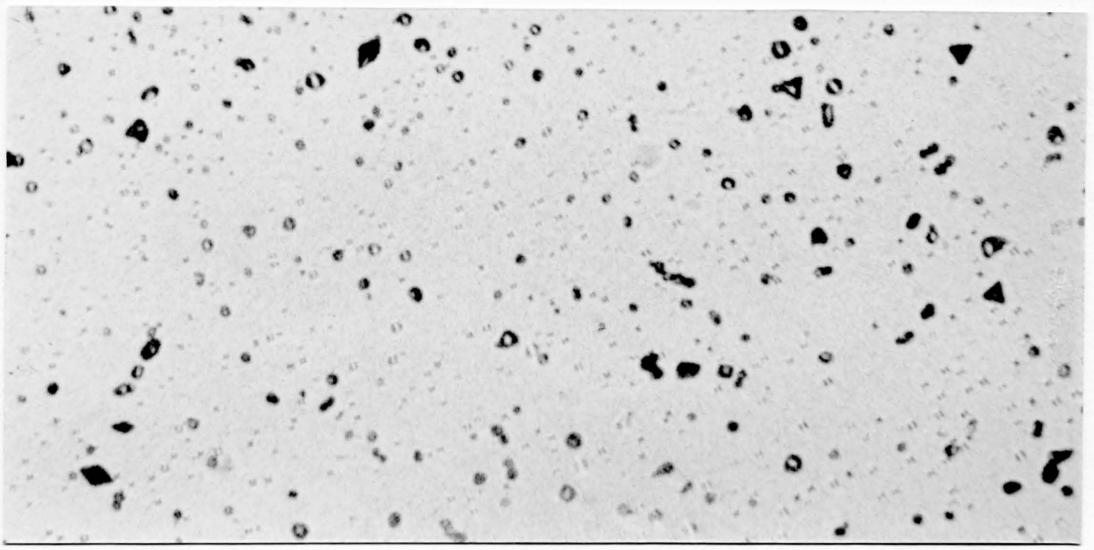

Figure 8. Ammonia Crystals Formed at -98°C.

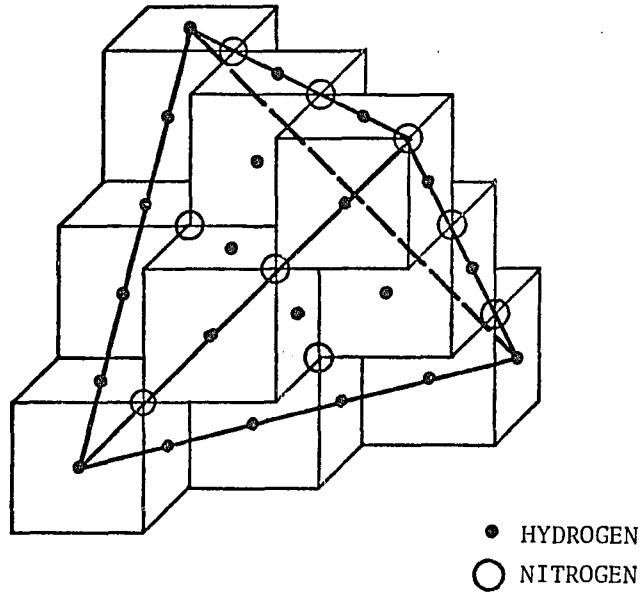

Figure 9. Crystal Structure Compared with Primitive Cubic Lattice Structure.

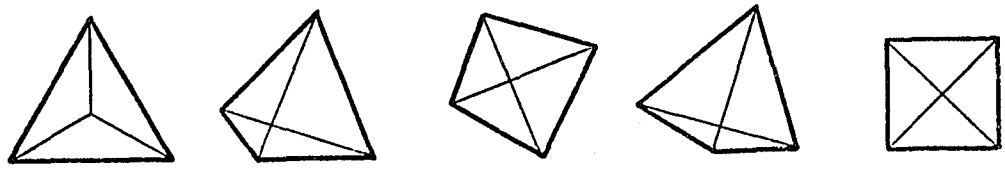

Figure 10. Four-sided Pyramid Crystals as Seen in a Variety of Orientations.

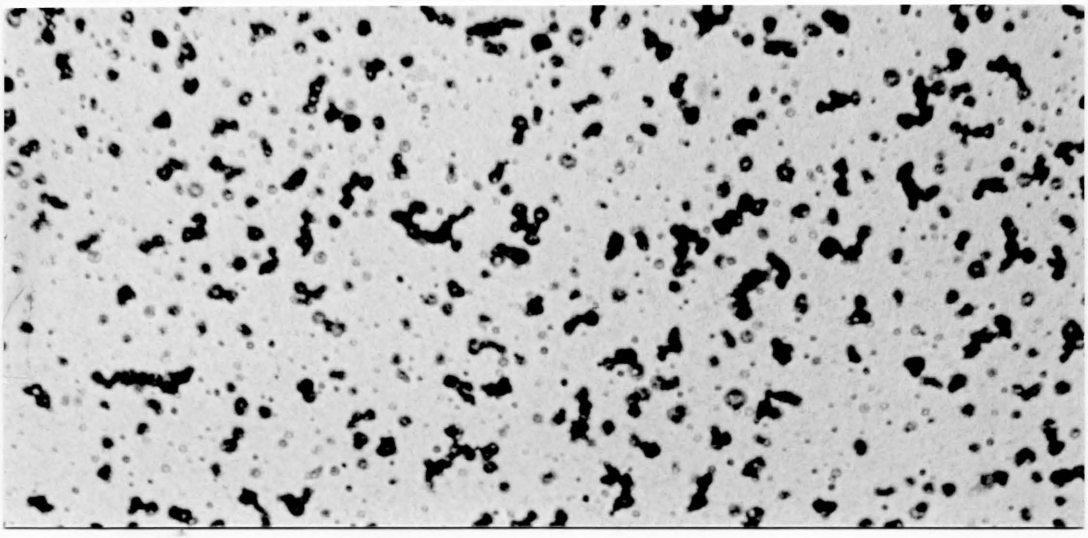

Figure 11. Ammonia Crystals Formed at -117°C.

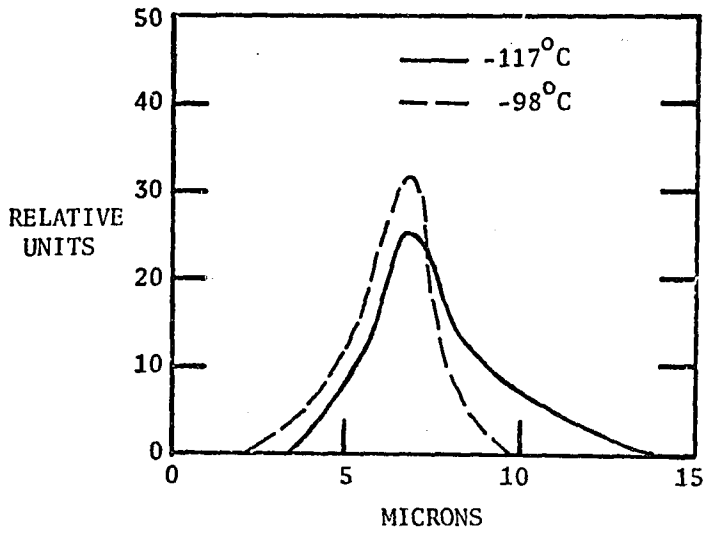

Figure 12. Size Distribution of the Maximum Dimensions of the Ammonia Crystals Illustrated in Figures 8 and 11.

CHAPTER 4

MEASUREMENT OF LIGHT SCATTERING CHARACTERISTICS

The Pioneer 10 and 11 spacecraft polarimeters returned images of Jupiter at a variety of Sun-Jupiter-probe scattering angles. Measurements of Jupiter from the earth are limited to backscattering angles where the light has been turned through an angle of at least 168°. Images of the crescent Jupiter returned by the polarimeters contained information on the light scattering of clouds at previously unobtainable angles down to 32°, a forward scattering region. From this information, Tomasko, West, and Castillo (1978) have deduced the single-scattering phase function appropriate to the cloud particles of the upper cloud decks. This phase function is a measure of the total intensity scattered by a parcel of cloud particles as a function of angle. It does not contain information about the polarization of the scattered light. This property is largely described by the "degree of linear polarization" function (of angle) which was estimated from Pioneer data by Stoll (1980). The measurements acquired in this laboratory research are intended to complement the Pioneer data as closely as possible. Cloud particles manufactured in the laboratory are characterized as to their single-scattering phase function and their degree of linear polarization function.

Single Scattering and Linear Polarization Functions

The single scattering phase function for a particle is a measure of the intensity, i.e., luminance, of the particle as seen from different angles when illuminated with unpolarized light. Mathematically the luminance L of light scattered by a particle is given by (Hansen and Travis, 1974):

$$L(\theta,\phi) = Q_{sca} \cdot E \cdot G \cdot \frac{P_{\parallel}(\theta,\phi)}{4\pi} \frac{\text{watt}}{\text{steradian particle}} , \quad (1)$$

E = Irradiance incident upon particle (watts/mm^2)

G = Geometric cross section particle presents to the illumination (mm^2/particle)

Q_{sca} = Ratio of scattering cross section to geometric cross section. Typically 2 for particles large compared to the wavelength of light.

$P_{\parallel}(\theta,\phi)$ = Single scattering phase function

θ = Scattering angle (forward scatter = 0°)

ϕ = azimuth angle.

The phase function is normalized in the following manner:

$$1 = \int_{\text{sphere}} P_{\parallel}(\theta,\phi) \frac{d\Omega}{4\pi} . \quad (2)$$

In this study measurements of phase functions were taken at scattering angles from 10° to 170°. The phase function is normalized to unity over this angular range to avoid an uncertain extrapolation of the phase function outside this range, particularly near the powerful

forward scattering direction. The particles were assumed to be randomly oriented (no ϕ dependence of scattering function) in performing the integration. This normalization is expressed below:

$$1 = \frac{1}{2}\int_{10°}^{170°} P_{\parallel}(\theta) \sin\theta \, d\theta \quad . \tag{3}$$

Usually a cloud of particles is measured. If the cloud is thin and multiple scattering and obscuration effects can be ignored, the radiance (or luminance) of the scattered light from the cloud will be given by:

$$L = Q_{sca} \cdot G \cdot \rho \cdot t(\theta) \cdot E \cdot \frac{P_{\parallel}(\theta,\phi)}{4\pi} \quad , \tag{4}$$

where

$t(\theta)$ = thickness of cloud as seen from observation point (nm)

ρ = density of clouds (particles/mm^3).

The analysis above ignores the polarization nature of the scattered light. The radiation scattered by a particle illuminated with unpolarized light is in general composed of an unpolarized fraction and an elliptically polarized fraction. The degree of linear polarization is a partial measure of the polarization properties. If the plane defined by the source, scatterer, and receiver is horizontal, the degree of linear polarization is given by:

$$\frac{I_r(\theta) - I_\ell(\theta)}{I_r(\theta) + I_\ell(\theta)} \quad , \tag{5}$$

where

$I_r(\theta)$ = intensity of scattered vertically polarized light

$I_\ell(\theta)$ = intensity of scattered horizontally polarized light.

Appendix A contains the theory of the polarization measurement technique employed.

Experimental Approaches

The traditional approach to performing light scattering measurements has been to illuminate the crystal cloud with a laser beam and utilize collection optics, polarization analyzers, and detectors on the end of a long rotating arm for measuring the scattering from 10° (forward scattering) to 170° (backscattering). As this rotation usually takes a minute or so, a fixed detector is required to monitor crystal density fluctuations. The positive aspects of this approach are high angular resolution, chart recorder compatible data rates, and the need to build and calibrate only one or two detectors. The major disadvantage is the necessity of maintaining stable clouds over long time periods. Also, the high angular resolution is quite often purposely reduced in data analysis to reduce the noise level of the measurement.

The approach utilized here employs an array of detectors at different scattering angles to take the place of the scanning arm. The instrumentation is more complex but the requirements on cloud stability are reduced since only fractions of a second are required for a

measurement. The increased data rate mandates the use of a computer for data acquisition, and the increased number of detectors makes the cost of the most sensitive detectors available prohibitive. The most attractive feature of the array approach is that no moving parts are required and data taking and analysis can be accomplished quickly by the push of a button. Detector calibration is more critical as the relative outputs of detectors at two different angles are compared in computing the phase function.

Description of Scattering Machinery

The number of detectors used in the array described here was fifteen, providing coverage from 15° to 165° scattering angles at increments of 10° (with the exception of 85°, which was blocked by a chamber internal structure). This angular resolution is adequate for comparison to the Pioneer data and is quite adequate for use in radiative transfer calculations that involve substantial multiple scattering. The scattering measurement apparatus is diagrammed in Figure 13. Figure 14 contains photographs of the actual structure.

Vertical polarized 6328Å laser light passes through a photoelastic modulator and then into a beam expander. The light beam is truncated by a centered three millimeter diameter hole before entering the chamber to provide a more uniform cross section. The beam passes through two curved cylindrical windows, traverses the scattering region, and is absorbed in a simple, blackened, cylindrical light trap. Cloud particles in the scattering region scatter light back out through the curved cylindrical windows to the fifteen lens-detector combinations.

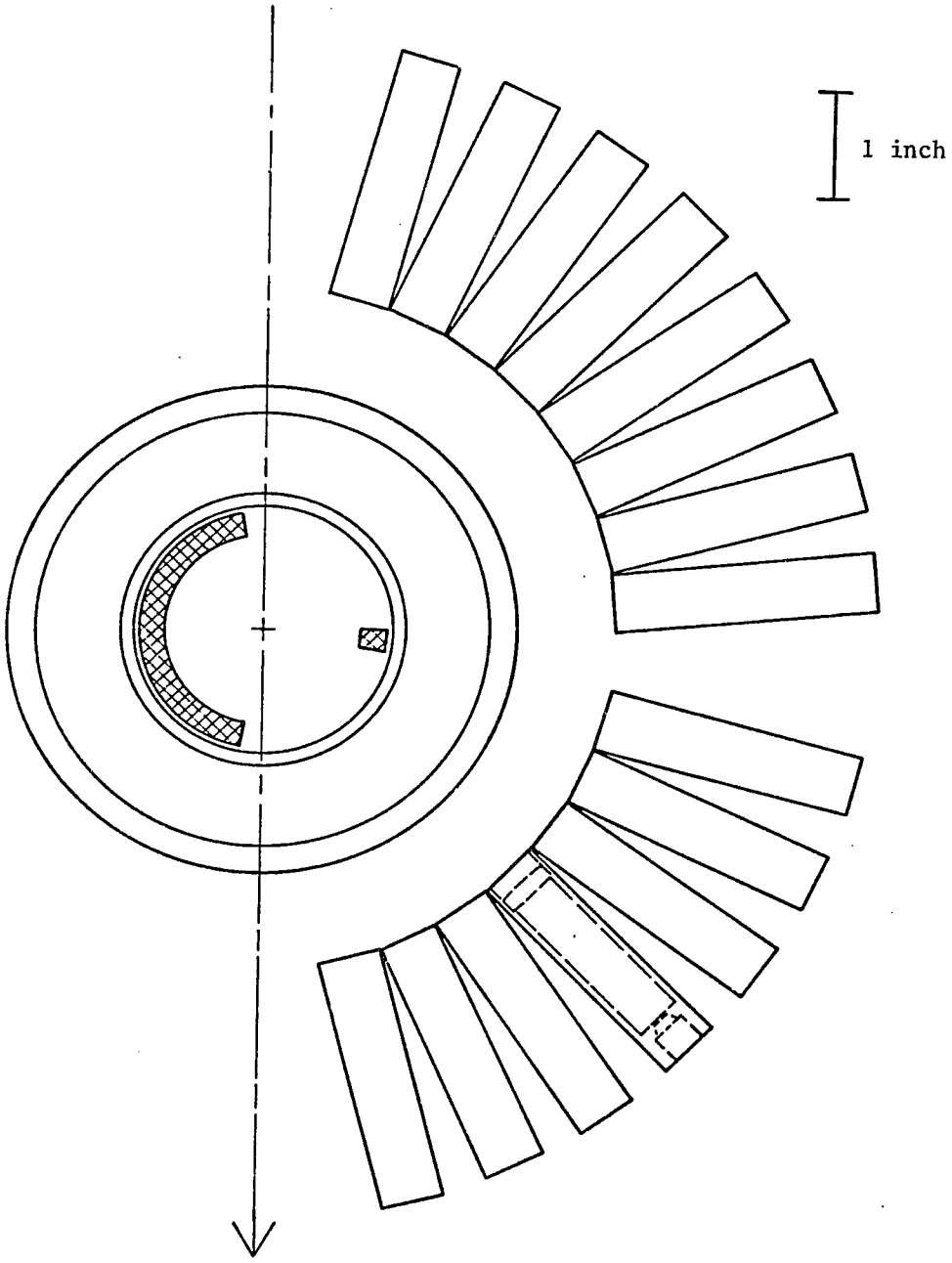

Figure 13. The Scattering Measurement Apparatus.

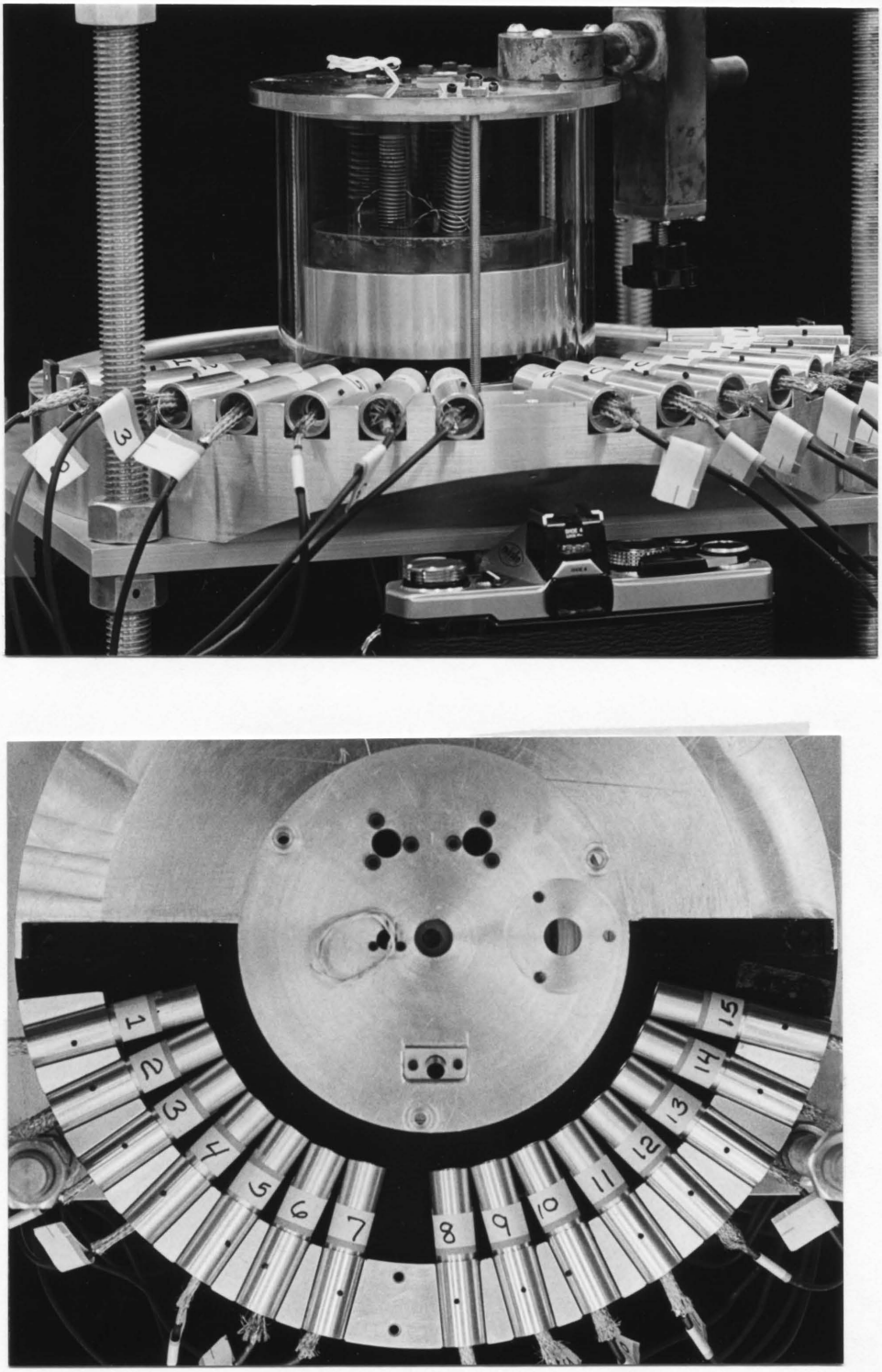

Figure 14. Two Views of Cold Chamber Surrounded by Detector Tubes.

Each lens serves to limit the angular acceptance of the scattered light and also to focus the scattering region onto a field stop. This field stop limits the field of view of each channel to a fraction of the illuminated cloud and provides for a common field of view, within limits, for all channels. A GaAsP photodiode is located a slight distance behind each field stop and is slightly underfilled by the illumination to allow for detector misalignment in its case. The detector outputs are relayed to an array of preamplifiers using shielded cables. The FET preamplifiers convert the current outputs of the detectors to voltages compatible with the remainder of the data acquisition system.

The lens-detector system employed here is drawn in Figure 15. The interior of the mounting tube is blackened, as is the front face of the field stop. The shallow curvatures of the lens surfaces coupled with the inherent insensitivity of the detector responsivity to polarization makes this combination insensitive to the polarization of the incoming light to less than one percent (difference in responsivity between unpolarized and polarized light).

Data Acquisition

The computer controlled data acquisition is illustrated in block form in Figure 16. The heart of the system is a Radio Shack TRS-80 microcomputer and its right arm is an instrumentation interface sold by Applied Micro Technology. The interface box contains a 12 bit analog to digital converter coupled to a 16 channel multiplexer along with 48 bits of parallel input/output (PIO) lines. The 15 detector preamplifier outputs are connected to the multiplexer. Eight bits of the

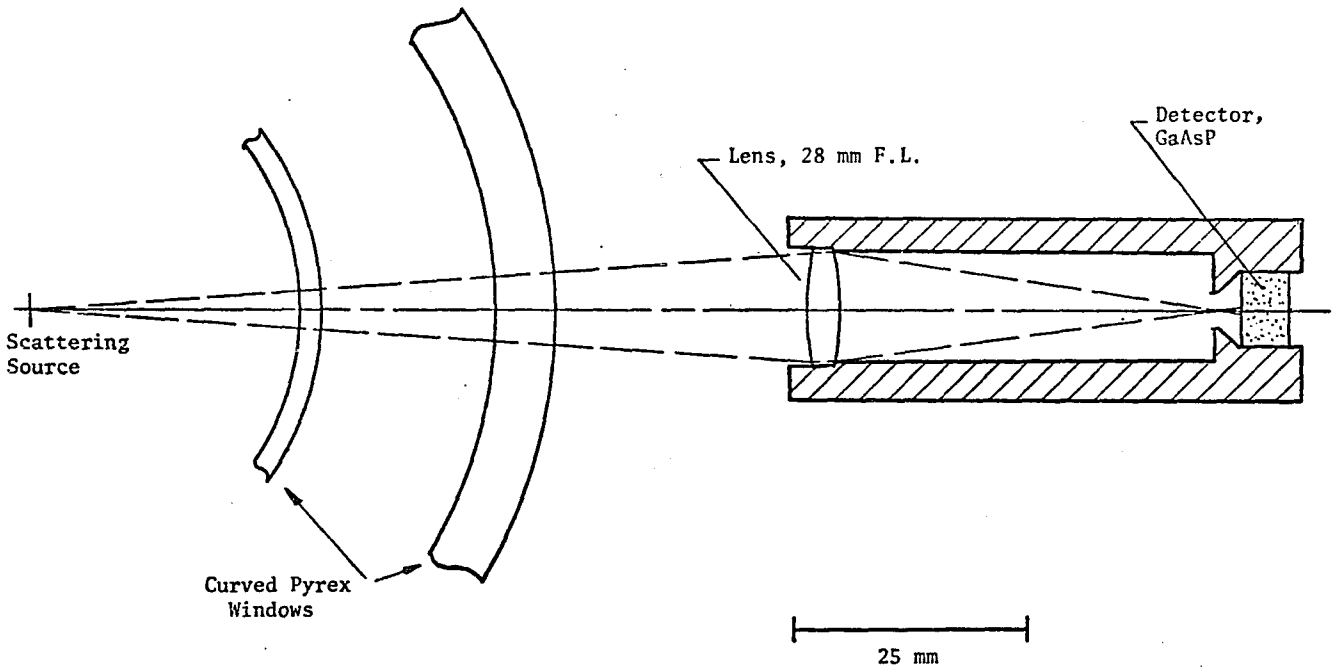

Figure 15. Optical Channel Configuration.

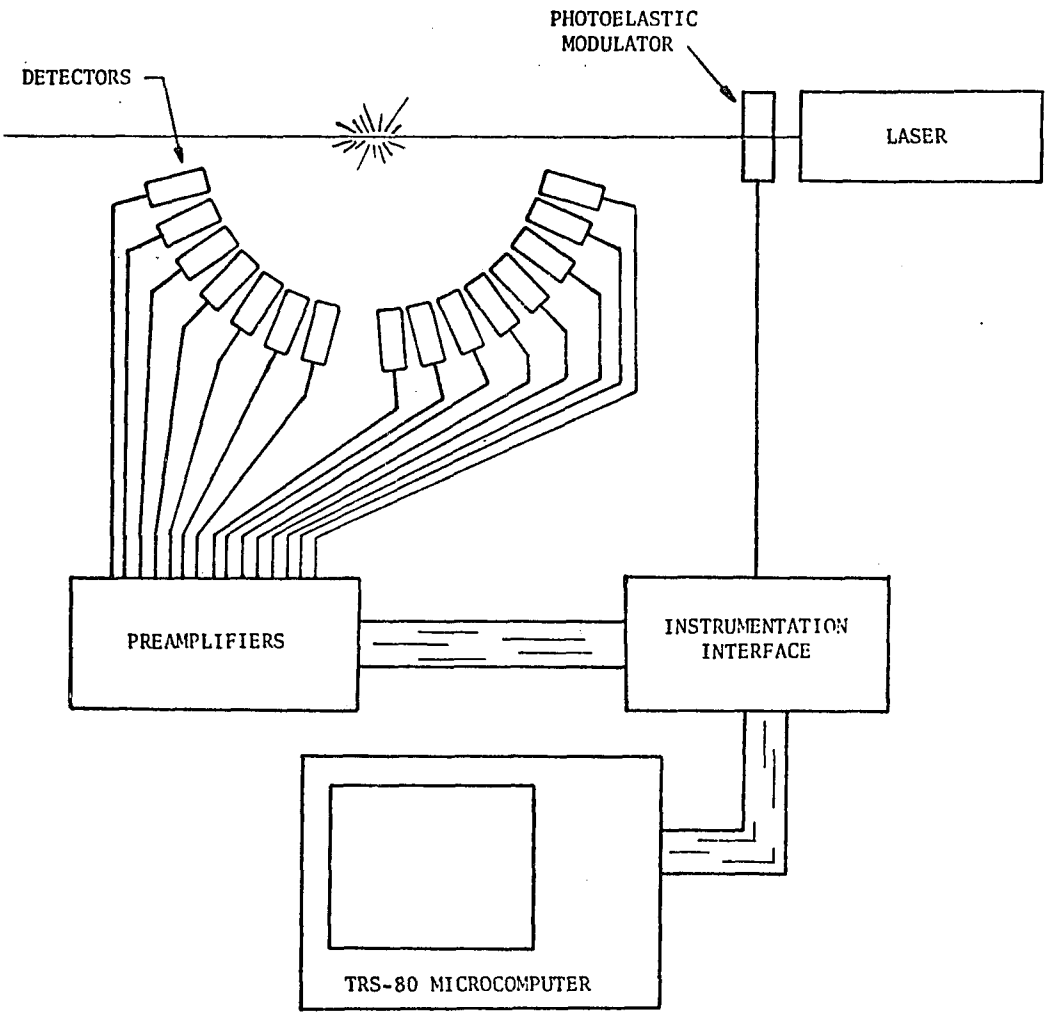

Figure 16. Data Acquisition System.

PIO lines feed into a digital-to-analog converter which sends an analog level to the photoelastic modulator controlling its drive level. (The photoelastic modulator and its operation are described in Appendix B.) The computer system makes possible rapid control of the data taking process. Initially the photoelastic modulator is on, depolarizing the vertically polarized laser beam. All 15 detector outputs are sampled sequentially and this is repeated four times, each repetition following the previous one by 1/240 second. The four samples for each detector channel are added together, a technique which greatly suppresses 60 hertz and 120 hertz pickup. After the sampling period for unpolarized scattering, a signal is sent to the photoelastic modulator which turns it off, allowing the laser beam to come through vertically polarized. A 1/30 second delay at this point allows the modulator to settle and the detector outputs, which have a five millisecond time constant, to reach their new levels. The data sampling process is then repeated for polarized illumination and the modulator turned back on to await the next data sampling. One-fifteenth second is required to completely acquire a data set. Thirty 12-bit words are generated and stored in computer memory for later analysis. In practice, 25 data sets are taken automatically over a period of five seconds to reduce the effect of crystal fluctuations on the polarization determination, as this determination requires the subtraction of two measurements taken 1/20 second apart (average). For this study, the data were averaged in the computer before storage on a disk for later analysis. The memory transfer rate from computer to disk was too slow to allow for storage of 25 sets of 30 data words.

All preamplifiers are dc coupled to the multiplexers and have output signals susceptible to temperature drift. For this reason, drift and offset must be subtracted from the data. When the moist wire heater is turned off, the crystals clear from the chamber in a matter of 30 seconds and a data set is taken. This data set contains the offsets due to amplifier dc drifts, light scattering off chamber parts and windows, and scattering from residual fogs in the chamber. These data are subtracted from the previous sets to yield the averaged signal data for the fifteen scattering angles.

Calibration

An accurate determination of the responsivity and polarization sensitivity of the lens-detector combination is important as the ratios of the channels to each other are used in determining the single scattering phase function of observed crystal clouds. The procedure adopted encompasses a closed circle in that a known scattering source was measured and the data compared with calculations done using geometry factors and detector responsivities.

The relative responsivity of each lens-detector combination was measured using the setup illustrated in Figure 17. The laser output was rendered unpolarized using the photoelastic modulator and expanded to a large beam. This beam was passed through a horizontal slit and onto a diffuse halon surface of high diffuse reflectivity. The height of the illuminated area on the white surface was fixed as 6 mm and the width at 30 mm. Each lens-detector combination was used to measure the irradiance of this rectangle from the prescribed distance. The field of view

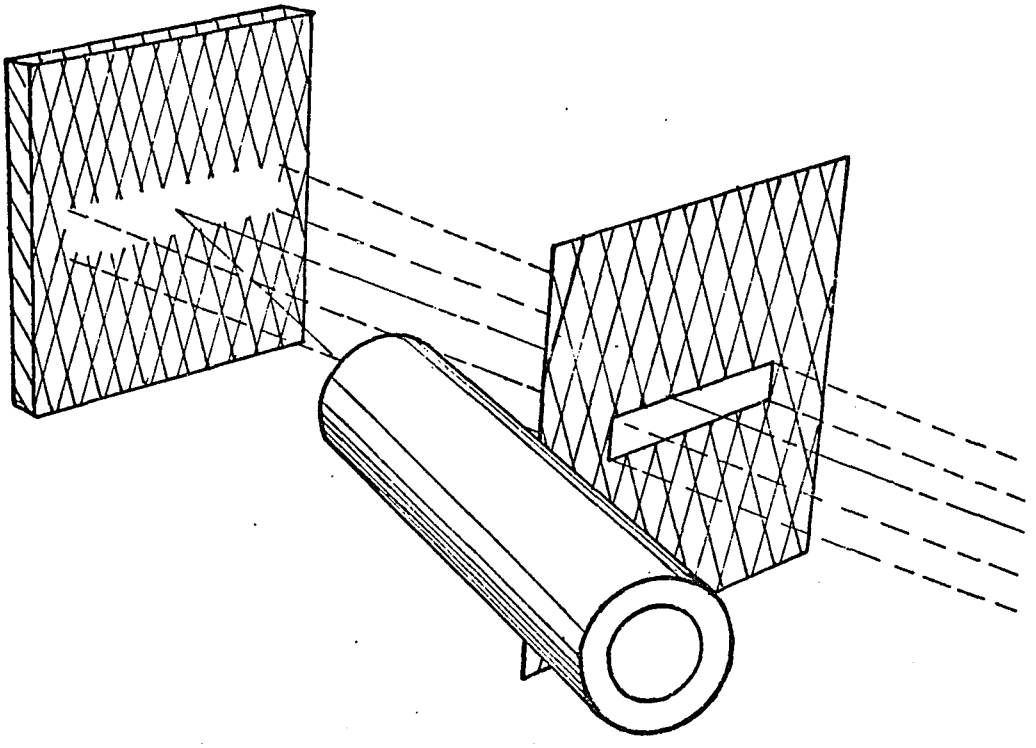

Figure 17. Responsivity Measurement Setup.

of each combination was two millimeters diameter on the screen, the illuminated area being made thicker to allow for misalignments. The illuminated area was designed to approximate the appearance of the laser beam passing through a cloud to minimize the effect any light scattering internal to the combination would have on the accuracy of the calibration. (Golden Rule #1: Calibrate the way you measure!) The responsivities are listed in Table 1.

Table 1. Calibration Factors.

Channel	Scattering Angle	Relative Responsivity	Geometry Factor	Response Speed Factor
1	15	.00687	2.342	.864
2	25	.00614	1.574	.880
3	35	.01	1.317	.877
4	45	.00903	1.258	.890
5	55	.925	1.173	.884
6	65	.881	1.0966	.846
7	75	.928	1.0341	.946
8	95	.862	1.003	.953
9	105	.924	1.0341	.943
10	115	.824	1.0966	.957
11	125	.873	1.173	.953
12	135	.913	1.258	.680
13	145	.862	1.317	.948
14	155	.859	1.574	.957
15	165	.911	2.342	.952

The lens-detector combination was expected to have little polarization sensitivity in its responsivity. This was verified using the system shown in Figure 18. The laser beam was passed through the photoelastic modulator and expanded to greatly overfill the lens of a combination. Attenuators were placed in the beam before the modulator to reduce the light level to an acceptable value. The modulator was turned on and off in a simulated data acquisition sequence and the detector output monitored to characterize the polarization sensitivity. The irradiance incident on the detector was constant, but the radiation changed in polarization nature. No polarization sensitivity was found that would result in an error in the determination of the degree of linear polarization of more than one percent. The data acquisition hardware was used to read detector outputs for all calibration operations.

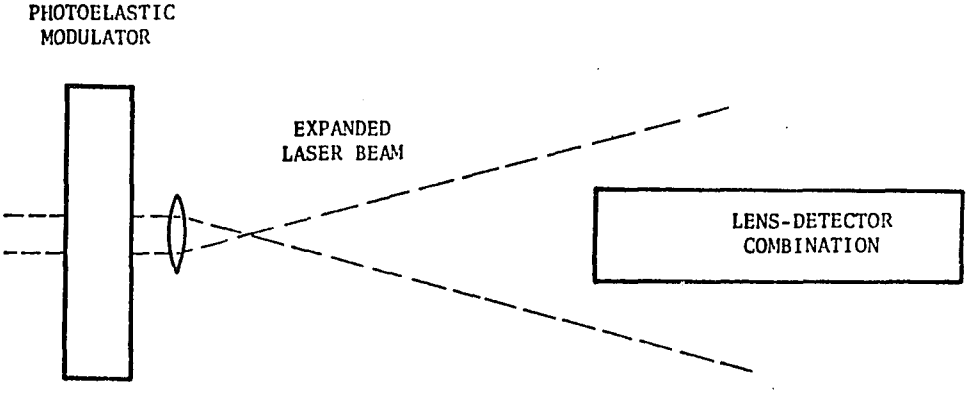

Figure 18. Measurement of the Polarization Sensitivity of the Lens-Detector Combinations.

The single scattering phase function is defined for individual crystals. A measurement here involves noting the intensity of scattered light from a beam passing through a cloud of crystals, introducing the situation that at very large or small angles the field of view will include a longer length $t(\theta)$ (Eq. 4) of the beam than at angles perpendicular to the beam. Also, the lenses used in this study are focused on the center of the scattering volume. Particles in the beam at different distances from the scattering volume center are detected with different efficiences. This problem is most acute for detector channels at scattering angles of 15° and 165°. These geometry factors must be accounted for in the data analysis. The technique for calculating these factors is explained in Appendix C.

All calibration factors are tabulated in Table 1, along with a response speed factor to be discussed in the next section.

Calibration Check

A check on the calibration of the scattering measuring instrument was performed to insure that no unforeseen errors were corrupting the results. A suspension of polystyrene spheres in water was used as the scattering medium. Two sizes of spheres were employed, 0.794 microns and 0.109 microns diameter. The small spheres behaved as Rayleigh scatterers and provided a check on the degree of linear polarization measurement. The larger spheres scatter light much more strongly into the forward direction and provided a better simulation of the phase function of the crystals. Lyn Doose of the Optical Science Center performed calculations of the scattering of these spheres using Mie theory and the

results were compared to the experimental data. The phase functions as measured and calculated are shown in Figures 19 and 20 and the degree of linear polarization functions for both large and small spheres in Figure 21. All phase function curves were normalized according to Eq. 3. Except for the additional backscatter measured for the 0.794 micron spheres, the fit is generally good and the differences that occur can be linked to sample preparation problems. This additional backscatter is caused by intense forward scattering from the large spheres illuminating the black backdrop surface that is observed by the backscatter channels. This stray light source is not severe enough to significantly degrade the measurements of the more strongly backscattering crystals.

Inspection of the figures reveals that the calculated wiggles in the single scattering phase function appear damped in the measurements, that the phase function for small spheres is too large in the forward direction, that the polarization for small spheres is too small in the forward direction, and that the polarization for large spheres is low in the backscattering hemisphere. All these problems can be ascribed to either impurities in the water or to clumping of the particulates being measured.

One instrumental error was found during the calibration process. The instrument's mode of operation involves making a measurement using unpolarized laser illumination, and then rapidly changing to vertically polarized illumination and taking a second measurement before the crystal species change significantly. Different channels were found to have different rates of adjusting to this change in light intensity (if a strongly polarizing sample was being measured). The lens-detector

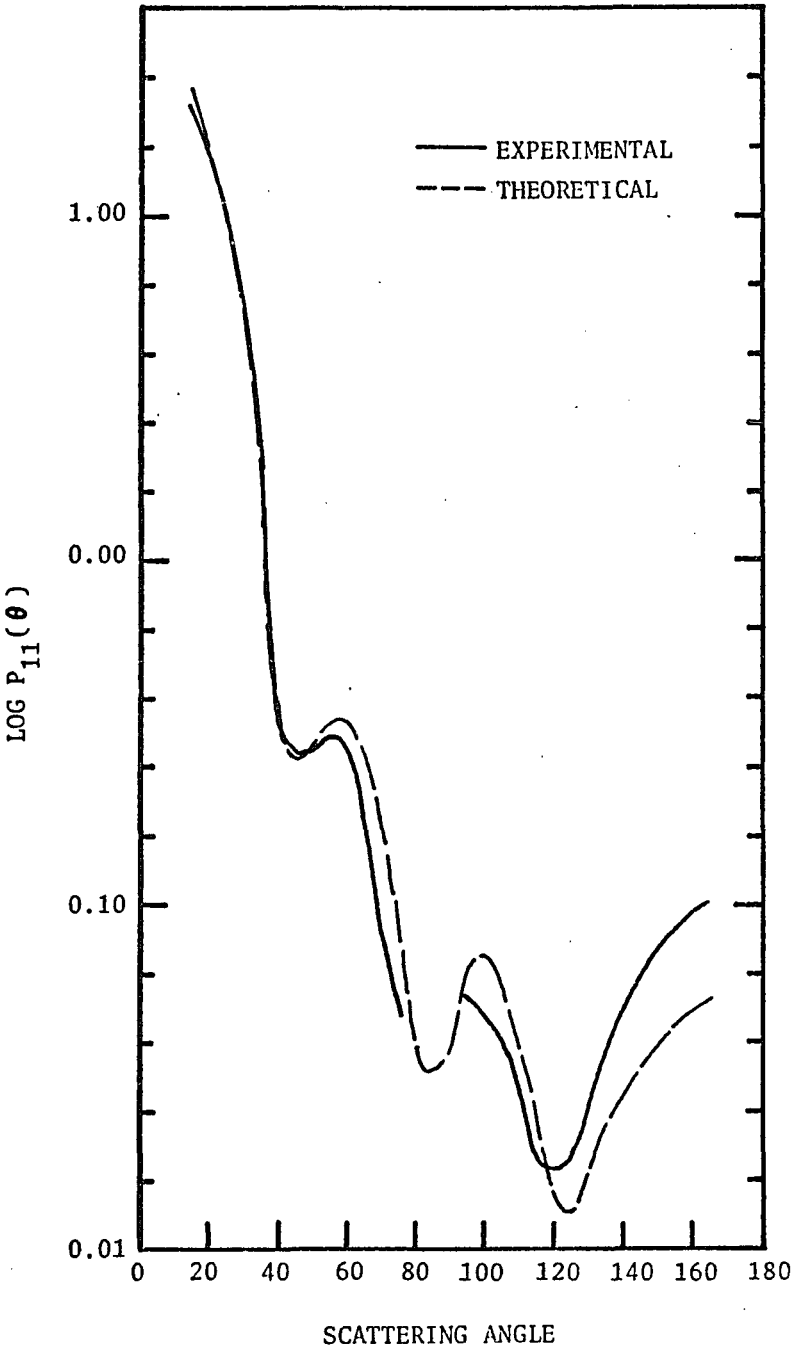

Figure 19. Single Scattering Phase Function as Calculated and Measured for 0.794 μm Polystyrene Spheres in Water.

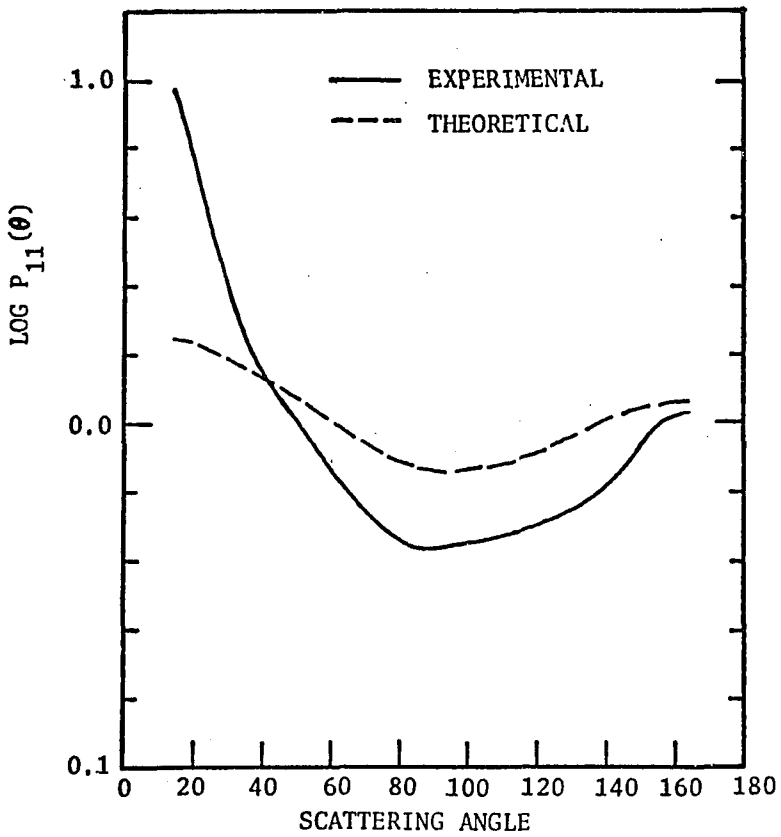

Figure 20. Single Scattering Phase Function as Calculated and Measured for 0.109 μm Polystyrene Spheres in Water. -- The sample was visibly contaminated, producing excess scattering in the forward direction.

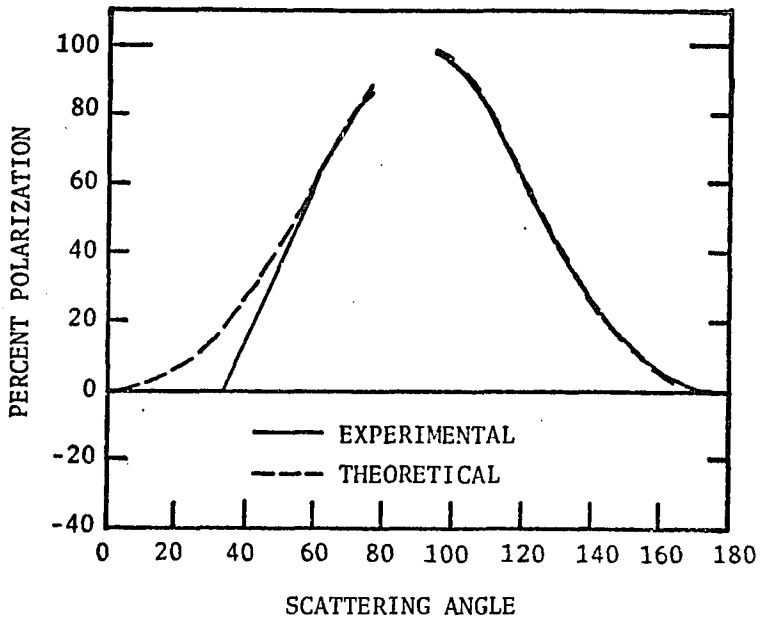

(a) 0.109 μm spheres

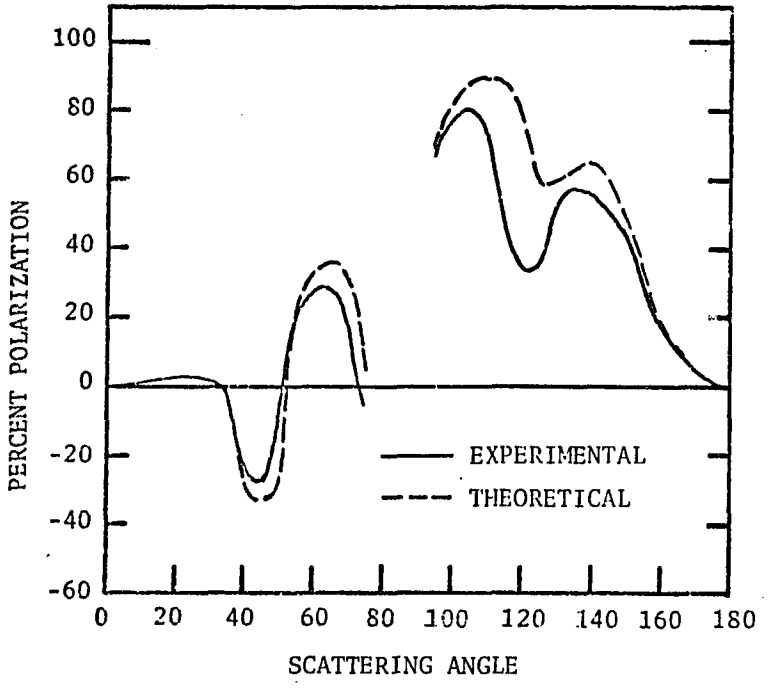

(b) 0.794 μm spheres

Figure 21. Degree of Linear Polarization Function.

combinations were placed back into the polarization sensitivity measurement setup (Figure 18) and a polarizer placed in front of each detector as it was tested. The setup then simulated a source that was 100% polarized. The percentage of total response was measured using the data acquisition hardware. The degrees of linear polarization measured varied from 68% to 95%, with the 68% being a singularly low reading. The measured responses are tabulated in Table 1. This sluggish response was corrected in the data analysis by dividing the measured polarization by the response factor, improving the theoretical to experimental fit to that illustrated in the previous figures.

The success of the measurement of the scattering functions for latex spheres in water indicates that no serious experimental errors are occurring. The measurement on the spheres is not meant to be a calibration, but rather a test for major experimental or computational errors.

CHAPTER 5

RESULTS OF SCATTERING EXPERIMENT

The apparatus described in the previous chapters was used to measure the scattering properties of ammonia and water crystal clouds. A cloud would be formed in the chamber and inspected visually to determine when its uniformity across the center of the chamber was adequate. When the uniformity became satisfactory, the computer would be initiated, and 25 sets of data taken in the following five seconds. A photograph of the precipitating particles would then be taken and a short description of the chamber conditions written. The computer would transfer the data to disk storage and print out a results summary within one minute of the data acquisition. If chamber conditions were still good, another data set would usually be acquired. The data stored on disk were analyzed after the data taking session was finished. The single scattering phase function was normalized from 10° to 170°. This was done to eliminate the need to extrapolate the measured data to 0°. Two different measurements of a phase function curve could then be compared without any uncertain extrapolation affecting the comparison by shifting one curve relative to the other.

Water Crystals

Good data were acquired for the water crystal clouds illustrated in Figures 4, 5, and 6. The single scattering phase functions measured

are shown in Figures 22 and 23 along with curves representing the results of Sassen and Liou (1979) renormalized as described in Eq. 3. The cloud measured by Sassen and Liou was formed at -12°C and contained plate crystals with an average maximum dimension of 3.5 μm. This modal size is similar to the clouds measured here, with the clouds formed at -39°C, -26°C, and -18°C having crystals with average maximum dimensions of 3.7 μm, 5.5 μm, and 8.5 μm respectively. The fit is very good, the most significant difference being the higher backscatter measured here. The normalization procedure forces the curves to match in an average sense in the forward scattering direction as the contribution to the integral of Eq. 3 is greatest from this region. Note that the curves measured here agree well at the 165° backscatter angle and that the cloud of small particles has less sidescatter than the clouds of larger particles. This latter trend is opposite that observed for water spheres of similar size. Also, evidence of an increase in the single scattering phase function near the 22° halo angle is apparent in the curve for crystals of mean size 8.5 μm. Smaller crystals do not have this feature. Sassen and Liou noticed similar features in their data.

The degree of linear polarization functions for the water crystal clouds described earlier are given in Figure 24, along with Sassen and Liou's measurements. It is apparent that Sassen and Liou's results appear to differ by a shift of +10% from measurements made here of 3.7 μm crystals. The technique employed by Sassen and Liou required the subtraction of two normalized functions derived from measurements made on the same cloud 3½ minutes apart. The measurements here required only five seconds to accomplish and were much less sensitive to slow

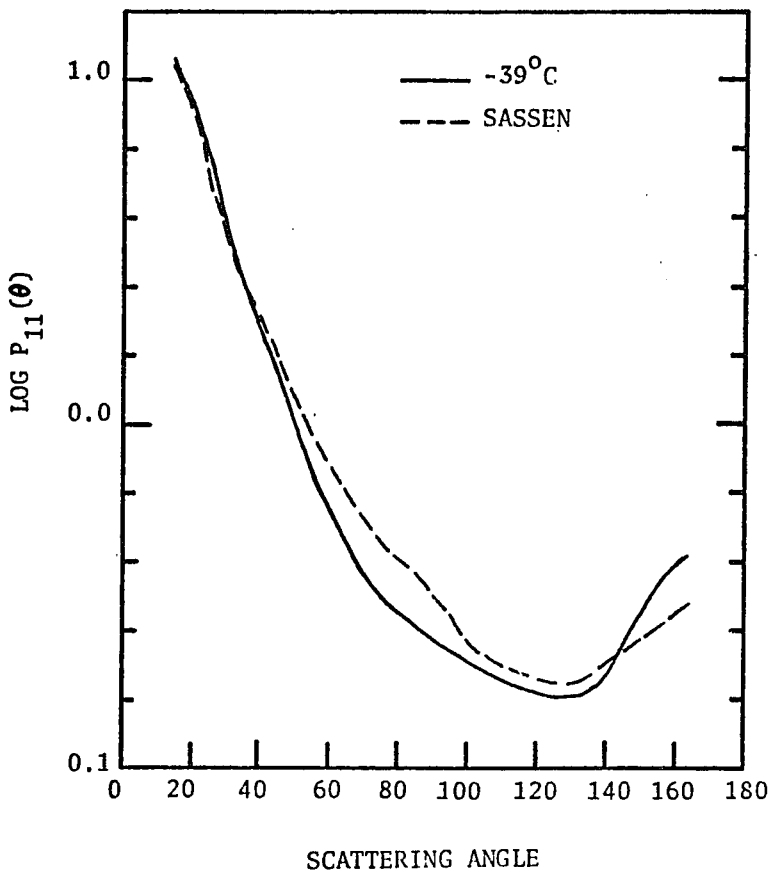

Figure 22. Single Scattering Phase Function of the Data of Sassen and Liou (1979) and for Measurements Here of 3.7 μm Diameter Crystals at -39°C.

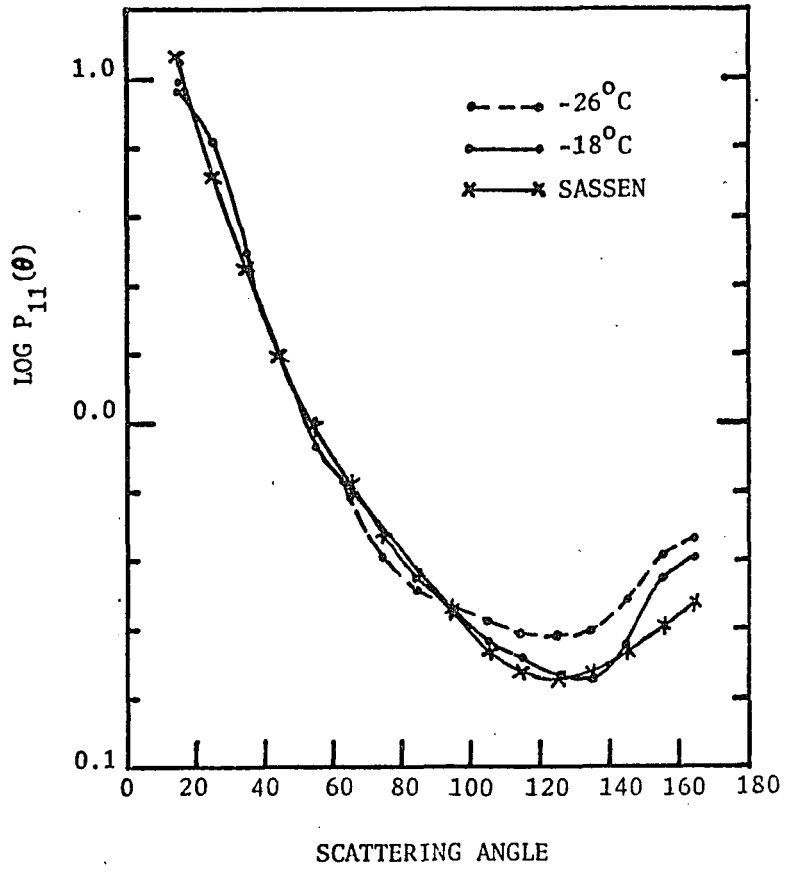

Figure 23. Single Scattering Phase Function for the Data of Sassen and Liou (1979) and Measurements Here of Plate Crystals Found at -26°C and -18°C.

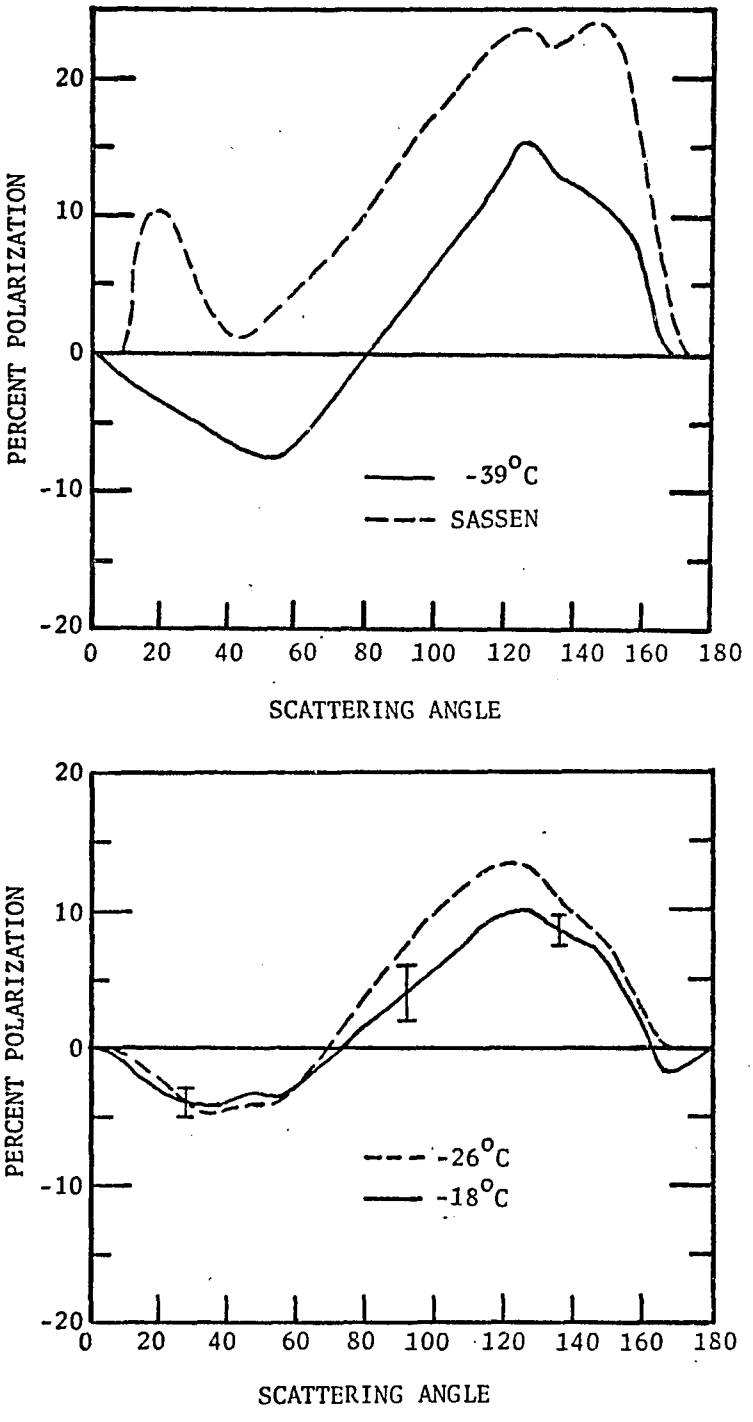

Figure 24. Degree of Linear Polarization for Water Crystal Clouds as Measured Here and by Sassen and Liou (1979).

fluctuations in cloud properties. Sassen (private communication, Meteorology Department, University of Utah, 1980) has stated that a 10% shift of the entire polarization curve illustrated in Figure 23 would be compatible with his measurement technique. With such a shift only the point at 10% would be in significant disagreement.

It should be noted here that digitization error, detector and electronic noise errors, and calibration errors were all insignificant compared to the crystal production problems in these measurements. The most perturbing problem in the determination of the single scattering phase functions and linear polarization functions was nonuniformities in the density of the crystal cloud along the laser beam. These nonuniformities were sometimes so localized as to present an empty region 3 mm wide anywhere in the beam (usually in the chamber center). Quite often the distribution was lopsided. Data were only taken when the cloud in the chamber appeared uniform, but 20% to 30% fluctuations could have easily occurred unnoticed. Data point errors in the forward scattering direction (15°-55°) will not affect the single scattering phase function results strongly in this region as these points are normalized in an average sense in the data reduction. The sidescatter portion of the phase function is more affected by inhomogeneities in the crystal cloud. Error estimates can be made from an examination of multiple data sets on clouds acquired in this study. The uncertainty in the phase function is ±5% in the forward scatter directions, ±10% in the side scatter, and ±30% in the backscatter direction. The reason for the poor repeatability in the backscatter channel is not known, but it appears to be associated with the particle clouds and not the equipment.

Errors in the degree of linear polarization measurement can occur if the density of crystals changes in the 1/15 second required to make a measurement. Twenty-five data sets are taken in five seconds to reduce this fluctuation error to less than ±1.5% at any angle.

Ammonia Crystals

The measurement of the light scattering characteristics of ammonia crystal clouds was subject to the same problems as water crystal clouds. The single scattering phase functions measured for the crystal particles illustrated in Figures 8 and 11 are shown in Figure 25. The backscatter peak is about three to four times greater than observed for water crystals. This backscatter peak is most likely due to the ammonia crystals possessing a crudely spherical shape. Spheres in the same size range possess large backscatter peaks. Water crystals, notably plate crystals, are not at all spherical. The forward scattering has a slope almost identical to that for water crystals.

The degree of linear polarization functions for the same two ammonia crystal clouds are illustrated in Figure 26. Very little polarization is observed. No cloudbow feature common for spherical particles is observed as this feature quickly disappears with a slight departure from sphericity of the scattering particles.

The error in the single scattering phase functions for ammonia is typically ±10%. The backscatter angle scattering was more repeatable than in the case of water crystals.

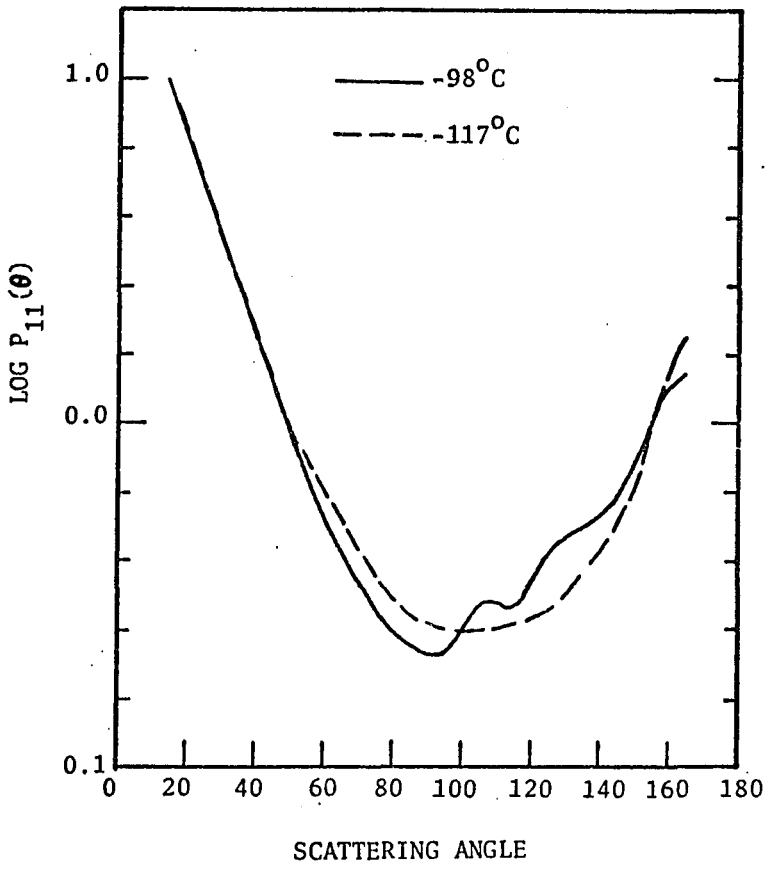

Figure 25. Single Scattering Phase Function for Ammonia Particles Formed at Two Different Temperatures.

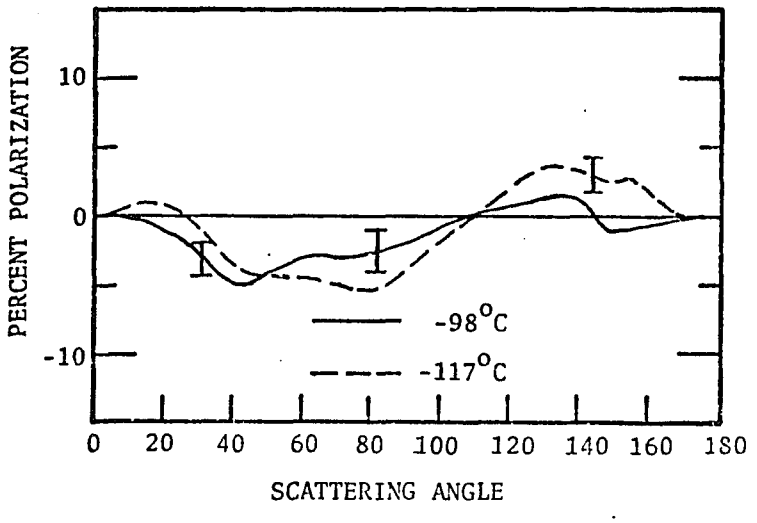

Figure 26. Degree of Linear Polarization Functions for Two Crystal Distributions.

CHAPTER 6

COMPARISON OF SCATTERING MEASUREMENTS WITH JUPITER DATA

The hope at the beginning of this research was that laboratory measurements of the light scattering of ammonia crystals would agree with the single scattering phase function derived from Pioneer 10 measurements of Jupiter by Tomasko, West, and Castillo (1978). In Figure 27 typical measurements of laboratory clouds of ammonia crystals and water crystals are compared with the phase function that yielded the best fit to the Jupiter data. The function lies between the ammonia and water crystal cloud phase functions. The upward pointing arrows represent the angles at which analyzed Pioneer measurements are available. It should be noted that some measurements of ammonia crystal clouds formed at -104°C were within ±10% of the Jupiter results. The typical cloud, however, scattered the laser beam as illustrated. Ammonia and water crystal clouds often had less backscatter than illustrated, but seldom more. Less measured backscatter is also often associated with poor cloud uniformity, making a choice of an "average" phase function difficult. It is possible that the scatter in the measurements is not necessarily caused by poor cloud uniformity, but rather is an actual variation in the scattering properties of the crystal species under observation. More experiments with careful control over the crystal conditions will help resolve this issue.

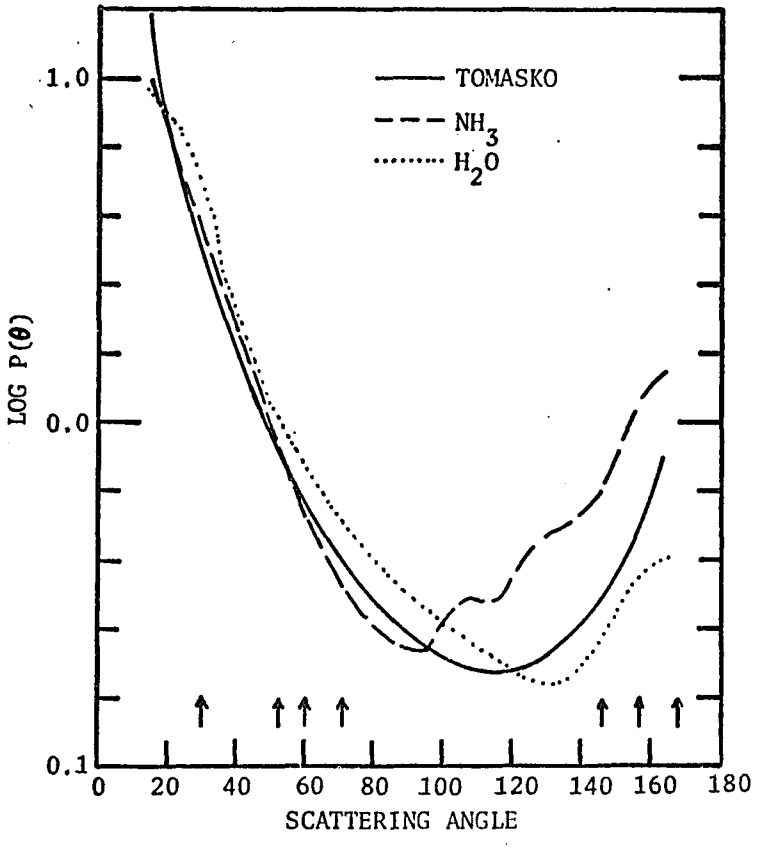

Figure 27. Intercomparison of Measurements of Ammonia and Water Crystal Clouds with Phase Functions Derived for Jupiter by Tomasko, West, and Castillo (1978).

It was observed in data taking and analysis that smaller crystals tend to have phase functions with less sidescatter and backscatter than the crystals analyzed here. It is possible that manufacture and measurement of smaller crystals will yield data more similar to the Jupiter results.

The water and ammonia crystal cloud scattering properties are obviously different for both the phase function and linear polarization function (Figure 28). This fact gives hope to the possibility of remote identification of cloud particles for the outer planets. Work is continuing here to improve the knowledge of the scattering properties of ammonia and water.

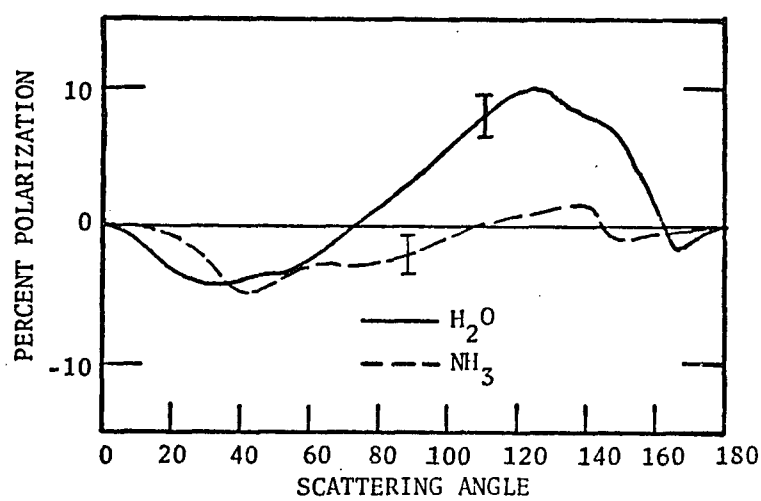

Figure 28. Intercomparison of Polarization Measurements of Ammonia and Water Crystal Clouds.

CHAPTER 7

CONCLUSIONS AND FUTURE WORK

This experimental research was concerned with developing equipment and techniques for growing, photographing, and measuring the scattering properties of H_2O and NH_3 crystal clouds. The equipment was used to perform initial measurements on crystal clouds to verify the achievement of these goals. There is a need to further improve the instrumentation as is typical of all experimental researches. The equipment has proved capable of accurate measurement of the degree of linear polarization for clouds but has been found to suffer from an unquantified knowledge of the cloud uniformity in the beam in the determination of the phase function. Two approaches can be pursued to reduce this uncertainty. More effort could be put into making stable, uniform crystal clouds or a silicon reticon diode array could be used, with an imaging lens, to measure the cloud nonuniformities by measuring the light scattered, at a fixed angle, along the length of the beam. The second approach is necessary to determine the success of the first, and should be implemented.

A heater would be valuable near the microscope cover glass. Many times difficulty was encountered in determining the crystal species falling when debris left from a data run five minutes before still lay on the cover glass. A heater would be employed to evaporate particle debris.

A modification of great use to planetary astronomers searching for matches to cloud scattering functions would be the inclusion of a laser emitting at a wavelength near 0.45 microns. Scattering measurements made on a cloud at red and blue wavelengths nearly simultaneously would add to the useful data. (Pioneer 10 and 11 measurements were made in both red and blue light.)

More experimentation should be performed to improve the control over the crystal clouds. Helium or hydrogen should be used as the carrier gas to determine if the crystal shape has a dependence on the gas thermal conductivity. Greater accuracy of scattering measurement will most likely be required to quantify the differences in the scattering functions of crystals formed under different circumstances.

APPENDIX A

THEORY OF THE SCATTERING MEASUREMENT

The light incident upon the clouds of Jupiter is sunlight and is completely unpolarized. The light scattered from the clouds may achieve some polarization. An aspect of this polarization easily measured is the degree of linear polarization, defined by:

$$\frac{\langle a_r^2 \rangle - \langle a_\ell^2 \rangle}{\langle a_r^2 \rangle + \langle a_\ell^2 \rangle} \quad .$$

The convention employed by van de Hulst (1957) is used here. The plane of scattering is defined by three points; the light source, the scattering region, and the detector. The component of the light having its E-vector perpendicular to the plane of scattering is denoted by a subscript r; the component parallel with a subscript ℓ. A monochromatic wave emerging from the scattering region can be described in terms of these two components.

$$E_\ell = a_\ell \, e^{-i\varepsilon_1} e^{-ikz + i\omega t} \quad ,$$

$$E_r = a_r \, e^{-i\varepsilon_2} e^{-ikz + i\omega t} \quad ,$$

$$\delta = \varepsilon_1 - \varepsilon_2 \quad .$$

The Stokes parameters are a convenient way of writing down the state of polarization of a light wave (or ensemble thereof). They are related to the E-vectors above by the following set of equations:

$$I = \langle a_\ell^2 \rangle + \langle a_r^2 \rangle \quad ,$$

$$Q = \langle a_\ell^2 \rangle - \langle a_r^2 \rangle \quad ,$$

$$U = \langle 2a_\ell a_r \cos \delta \rangle \quad ,$$

$$V = \langle 2a_\ell a_r \sin \delta \rangle \quad .$$

The Stokes parameters are usually written in vector form with the quantity I normalized to unity. Three pertinent examples are given:

Unpolarized Light

$$S = \begin{bmatrix} 1 \\ 0 \\ 0 \\ 0 \end{bmatrix}$$

Vertically Polarized Light

$$S = \begin{bmatrix} 1 \\ -1 \\ 0 \\ 0 \end{bmatrix}$$

Horizontally Polarized Light

$$S = \begin{bmatrix} 1 \\ 1 \\ 0 \\ 0 \end{bmatrix}$$

The scattering properties of a cloud, surface, or any other structure may be completely defined by finding the Mueller matrix representation. This Mueller matrix can be multiplied by the vector Stokes parameters for the input light to yield the Stokes parameters containing a complete description of the state of polarization of the scattered light. The Mueller matrix for ice crystals simplifies for randomly oriented ice crystals to the following form:

$$F = \begin{bmatrix} A_1 & B_1 & 0 & 0 \\ B_1 & A_2 & 0 & 0 \\ 0 & 0 & A_3 & B_2 \\ 0 & 0 & -B_2 & A_4 \end{bmatrix} .$$

Two examples of the use of this matrix form are given below:

UNPOLARIZED LIGHT INCIDENT UPON CLOUD

$$F \cdot S = \begin{bmatrix} A_1 & B_1 & 0 & 0 \\ B_1 & A_2 & 0 & 0 \\ 0 & 0 & A_3 & B_2 \\ 0 & 0 & -B_2 & A_4 \end{bmatrix} \begin{bmatrix} 1 \\ 0 \\ 0 \\ 0 \end{bmatrix} = \begin{bmatrix} A_1 \\ B_1 \\ 0 \\ 0 \end{bmatrix}$$

VERTICALLY POLARIZED LIGHT INCIDENT UPON CLOUD

$$F \cdot S = \begin{bmatrix} A_1 & B_1 & 0 & 0 \\ B_1 & A_2 & 0 & 0 \\ 0 & 0 & A_3 & B_2 \\ 0 & 0 & -B_2 & A_4 \end{bmatrix} \begin{bmatrix} 1 \\ -1 \\ 0 \\ 0 \end{bmatrix} = \begin{bmatrix} A_1 - B_1 \\ B_1 - A_2 \\ 0 \\ 0 \end{bmatrix}$$

Note that the degree of linear polarization (Eq. 5) for the light emerging from a cloud illuminated by unpolarized light is given by:

$$L.P. = -\frac{B_1}{A_1} .$$

The single scattering phase function is given simply by function A_1.

The scattering machinery described before has no polarization analyzers to affect the light after it is scattered and before it is detected. The degree of linear polarization is determined by measuring the total light scattered when the incident illumination is vertically polarized and comparing this amount to that which is scattered when the illumination is unpolarized. These two quantities, I_p and I_u respectively, yield the degree of linear polarization in the following equation:

$$L.P. = \frac{(A_1 - B_1) - A_1}{A_1} = \frac{I_p - I_u}{I_u} \quad . \tag{6}$$

This result follows from a consideration of the symmetries of the Mueller matrix for ice cloud crystals given on the preceding page.

APPENDIX B

THE PHOTOELASTIC MODULATOR

The photoelastic modulator was first applied to light scattering measurements by Hunt and Huffman (1974). The explanation of the modulator operation presented below follows their analysis closely, but to a slightly different end.

The modulator is pictured in Figure 29. It consists of a block of amorphous quartz about 70 mm long driven at its resonant frequency (fundamental mode) by a crystalline quartz transducer of very similar dimension. Close control of the mechanical tolerances on the length of these two blocks permits low power operation. A resonant acoustic

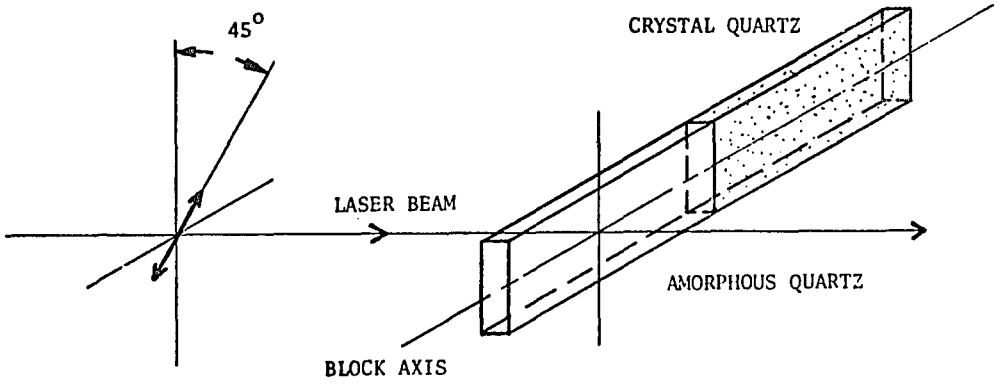

Figure 29. Schematic Diagram Illustrating Photoelastic Modulator Arrangement.

wave is produced in the amorphous quartz block, the wave producing a periodic stress birefringence in the material. This birefringence causes the index of refraction for light polarized parallel to the block axis (shown in Figure 29) to differ from that for light polarized perpendicular to this axis. The quartz behaves as a wave plate of rapidly oscillating (50 kHz) retardance. The phase retardance can be written as:

$$\delta = A \sin \omega t \quad ,$$

where A is related to modulator material, dimensions, and drive power, and ω is the angular frequency.

If the modulator block axis is at 45° to the axis of the polarization of the laser beam as illustrated in Figure 29, the Stokes vector for the laser light emergent from the modulator will be given by:

$$\begin{bmatrix} 1 \\ -\cos \delta \\ 0 \\ -\sin \delta \end{bmatrix} .$$

Cos δ and sin δ can be expanded in terms of Bessel functions to yield:

$$\cos (A \sin \omega t) = J_0(A) + 2J_2 (A \cos 2\omega t) + \cdots$$

$$\sin (A \sin \omega t) = 2J_1(A) \sin \omega t + 2J_3(A) \sin \omega t + \cdots$$

Note that if A is adjusted such that $J_0(A) = 0$, the Stokes vector for slow measuring devices ($<<$ 50 kHz) will become:

$$\begin{bmatrix} 1 \\ 0 \\ 0 \\ 0 \end{bmatrix}$$

This is the Stokes vector for unpolarized light. In practice, the retardance value A must be adjusted closely to 2.449, and the angle between the block axis and polarization direction set within a degree or two of 45°. An iterative adjustment approach has yielded good results here. The state of polarization of the emergent light was monitored with a polarizer and a polarization insensitive photodetector.

APPENDIX C

NORMALIZED ANGLE CALIBRATION FACTORS

A calibration factor for lens-detector combinations viewing a cylindrical volume of illuminated crystals must take into account the angle of view, beam diameter, field stop location and size, and the entrance pupil location and size for the system. This is demonstrated in Figure 30.

An image of the field stop in object space has been drawn to more clearly indicate the vignetting characteristics of the scattering volume. If a scattering point is to be detected, a line passing through it must also pass through both the field stop image and the entrance pupil. If the entire entrance pupil is not visible from the scattering point, that point is being vignetted. It can be seen in Figure 30 that unvignetted and vignetted regions exist. The solid angle of light from a scatterer captured by the lens varies within each of these regions.

A computer program was written to calculate the relative power scattered into detectors at different angles by an array of isotropic scatterers. The scatterers were arranged in a cubic lattice structure along the laser beam, the distance between adjacent lattice points being only 0.1 mm. The laser beam was set at 3 mm diameter, and the image of the field stop at 2 mm diameter. The entrance pupil lay 84 mm from the field stop image and had a diameter of 10.7 mm. The solid angle

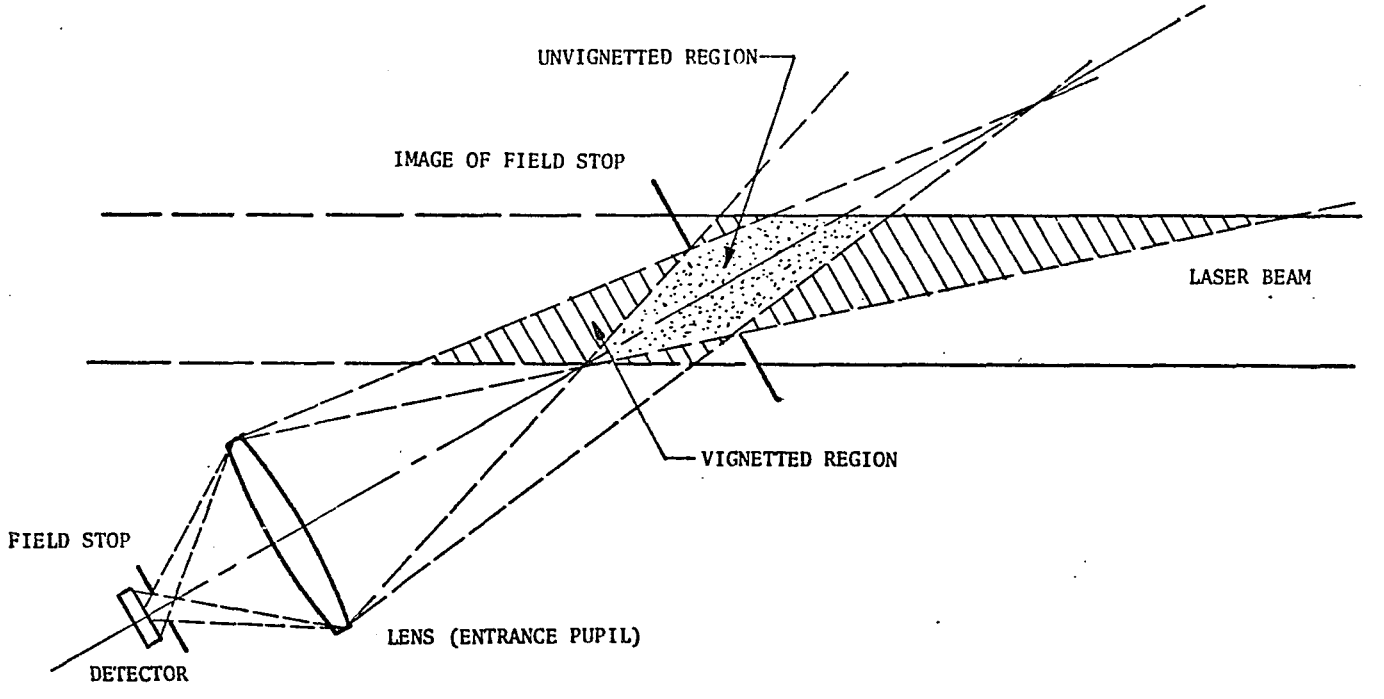

Figure 30. Geometry for Angle Factor Calibration.

subtended by the vignetted or unvignetted entrance pupil from each lattice point was calculated and summed over the length of the laser beam. The sums at each angle were normalized by dividing by the sum for a lens-detector combination at 90° to the beam. The quantity calculated was, in equation form,

$$\text{Angle factor } (\theta) = \frac{\sum_i \Omega_i(\theta)}{\sum_i \Omega_i(90°)} \quad .$$

The sum was over the lattice points. The results are tabulated in Table 2, and are symmetric about the perpendicular to the beam.

A further improvement in these factors is possible. An iterative technique could be employed by inputting the measured phase function into the program instead of an isotropically scattering phase function. This will change the results only slightly.

Table 2. Normalized Angle Calibration Factors.

Scattering Angle	Normalized Factor
90°	1.0000
85 or 95	1.0027
75 or 105	1.0341
65 or 115	1.0966
55 or 125	1.1735
45 or 135	1.2585
35 or 145	1.3171
25 or 155	1.5742
15 or 165	2.3417

LIST OF REFERENCES

Byers, H. R., Elements of Cloud Physics, University of Chicago Press, 1965.

Crystal Data: Determinative Tables (n.d.), Third edition, Vol. II. U.S. Dept. of Commerce, N.B.S., and Joint Committee on Powder Diffraction Studies, U.S.A., p. C-93.

Dugin, V. A., B. M. Golubitskiy, S. O. Mirumyants, P. I. Paramonov, and M. V. Tantashev, Optical properties of artificial ice clouds, Izv., Atmospheric and Oceanic Physics, Vol. 7, No. 8, 1971, pp. 871-877.

Hansen, James E., and Larry D. Travis, Space Science Reviews 16, 1974, pp. 527-610.

Huffman, Paul J., and William R. Thursby, Jr. (Captain, USAF), Light scattering by ice crystals, Journal of the Atmospheric Sciences, Vol. 26, Sept. 1969, pp. 1073-1077.

Hunt, Arlon J., and Donald R. Huffman, A polarization-modulated light scattering instrument for determining liquid aerosol properties, Proc. ICO Conf. Opt. Methods in Sci. and Ind. Meas., Tokyo, 1974 Japan. J. Appl. Phys., Vol. 14, 1975, Suppl. 14-1.

International Critical Tables (1928), McGraw-Hill Book Co., Inc., New York.

Lewis, John S., The clouds of Jupiter and the NH_3-H_2O and NH_3-H_2S systems, Icarus, Vol. 10, 1969, pp. 365-378.

Sassen, Kenneth, and Kuo-Nau Liou, Scattering of polarized laser light by water droplet, mixed-phase and ice crystal clouds. Part I: Angular scattering patterns, Journal of the Atmospheric Sciences, Vol. 36, 1979, pp. 838-851.

Stoll, Cliff, Polarimetry of Jupiter at Large Phase Angle, Ph.D. Dissertation, The University of Arizona, Tucson, 1980.

Sutherland, D. N., Chain formation of fine particle aggregates, Nature, Vol. 226, June 27, 1970, pp. 1241-2.

Tomasko, M. G., R. A. West, and N. D. Castillo, Photometry and polarimetry of Jupiter at large phase angles, Icarus, Vol. 33, No. 3, March 1978.

van de Hulst, H. C., Light Scattering by Small Particles, New York, Wiley, 1957, 470 pp.